T2K-NOvA acceptances

Edward Atkin[1] and Clarence Wret[2]

[1]Imperial College London (e.atkin17@imperial.ac.uk)
[2]Univeristy of Rochester (c.wret@rochester.edu)

January 2019

Contents

1 Background

This is a general note on T2K ND280 and SK acceptances as of 2019. The events entering the ND280 selections are selected in BANFF and MaCh3 and are fitted, and the events entering the SK selections are selected by the oscillation analyses in VALOR, p-theta and MaCh3. As such, it represents the current state of event selection for T2K oscillation analysis.

The hope is that these studies will not just be fruitful to gauge phase space differences for T2K and NOνA, but also to explore differences between ND280 and SK selections. This will be especially interesting for informing systematics and phase space mapping at ND280 and SK for the upcoming SK 2R selections—predominantly from 1π and multi-π events—which are being introduced later in 2019.

This note contains:

- Acceptance/efficiency maps for reconstructed selections, given a true selection
- Resolution for muons and pions (only at ND280)

2 Variables

The acceptance maps are given in true quantities. When plotting selected lepton or pion candidates we use the true particle of the candidate and its kinematics. The variables used to construct the different efficiency maps are

$$\begin{aligned} q &= (q_0, q_3) = P_\nu - P_\mu \\ Q^2 &= -q^2 = -\left(P_\nu - P_\mu\right)^2 \\ q_0 &= E_\nu - E_\mu \\ \vec{q_3} &= \vec{p}_\nu - \vec{p}_\mu \\ |\vec{q_3}| &= +\sqrt{\left(\vec{q_3}\right)^2} \\ W^2_{Obs} &= m_N^2 - Q^2 + 2q_0 m_N \\ y &= 1 - \frac{E_\mu}{E_\nu} \end{aligned} \tag{1}$$

where the W_{Obs} definition assumes the struck nucleon is on average at rest. This biases W_{obs} away from W_{True}. Particle variables, e.g. p_{lep}, $\cos\theta_{\nu,\pi}$, are defined in the lab frame. The acceptances are made in following 2D variables:

- $p_{lep}, \cos\theta_{lep}$
- $p_\pi, \cos\theta_\pi$
- $p_\pi, \cos\theta_{\mu,\pi}$
- q_0, q_3
- q_0, W_{Obs}
- E_ν, y

Attempts were made to bin into 3D, 4D and 5D histograms but MC statistics became an issue for finer binning. Hence we recommend using acceptance maps which match the variables to be plotted, e.g. if plotting $p_{lep}, \cos\theta_{lep}$ we recommend using the acceptance map in $p_{lep}, \cos\theta_{lep}$ and not one in q_0, W_{Obs}.

2.1 Binning

The binning for ND280 and SK was naively chosen and is not optimised. This is primarily because the backgrounds (true selections not equal to the actual selection) often populate a different phase space to the signal, and producing optimised binning for signal and background was outside the scope of this task. There was no effort to make binning dependent on selections for the same reason. The final chosen binning was

- p_{lep}: 300 bins, from 0 to 3 GeV/c; $\cos\theta_{lep}$: 200 bins, from -1 to 1
- p_{π}: 100 bins, from 0 to 1 GeV/c; $\cos\theta_{\pi}$: 100 bins, from -1 to 1
- p_{π}: 100 bins, from 0 to 1 GeV/c; $\cos\theta_{\mu,\pi}$: 100 bins from -1 to 1
- $\cos\theta_{\pi,\nu}$: 100 bins from -1 to 1; $\cos\theta_{\mu,\pi}$: 100 bins from -1 to 1
- q_0: 140 bins, from 0 to 1.4 GeV; q_3: 140 bins from 0 to 1.4 GeV/c
- q_0: 140 bins, from 0 to 1.4 GeV; W_{Obs}: 120 bins from 0.9 to 1.5 GeV/c^2
- E_{ν}: 200 bins from 0 to 2 GeV; y: 100 bins from 0 to 1

ND280 and SK acceptances were deliberately chosen to have matching binning.

Importantly, neither ND280 or SK event distributions or acceptance maps were weighted by any correction systematics (flux, cross-section or detector).

2.2 Closure tests

Closure tests of the procedure were performed, where the true events and corresponding acceptance maps were used to go back to the true spectrum of reconstructed events in various ND280 and SK selections. Since the same binning was used for the events and the acceptance maps, a flat ratio at exactly 1 is expected between the weighted true selected events and the reconstructed events.

Figure 1 shows the validation process for the true FGD1 CC0π distribution being weighted to the reconstructed FGD1 CC0π distribution. The closure test is complete and closes for all ND280 selections.

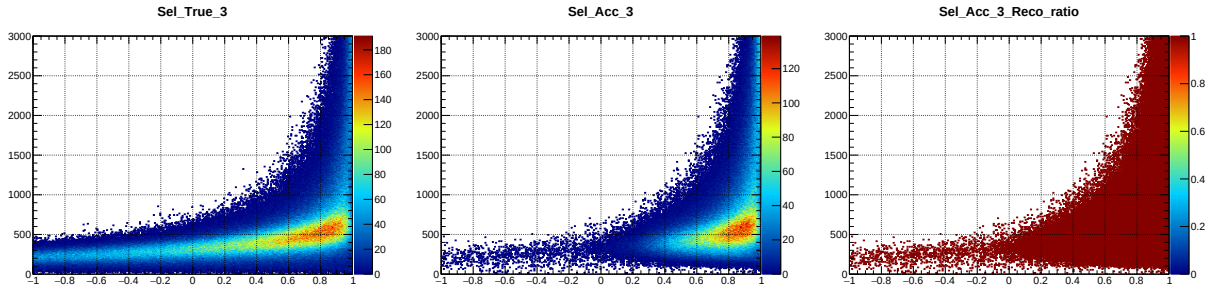

(a) Distribution of events passing FGD1 CC0π selection in truth

(b) Distribution of events passing FGD1 CC0π selection in truth weighted by the acceptance map, aiming to produce the reconstructed FGD1 CC0π spectrum

(c) Ratio of weighted true FGD1 CC0π spectrum to unweighted reconstructed FGD1 CC0π spectrum, completing the closure test

Figure 1: Closure test of acceptance maps and true events being able to reproduce the reconstructed distributions in $p_{Lep}, \cos\theta_{Lep}$

Similarly, a closure test was completed for SK. Figure 2 shows the closure test for true CC0π1μ events and the 1Rμ selection. The closure tests are complete for all SK selections.

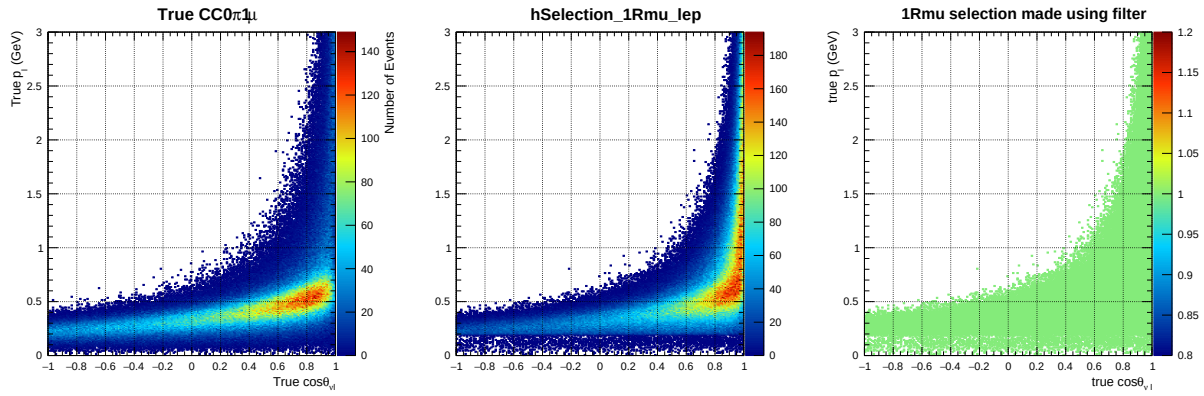

(a) True CC0π1μ events

(b) Distribution of events making the 1Rμ selection in truth weighted by the acceptance map

(c) Ratio of the weighted 1Rμ made with the acceptance map to the reconstructed 1Rmu distribution

Figure 2: SK closure test of acceptance maps and true events being able to reproduce the reconstructed distributions in $p_{Lep}, \cos\theta_{Lep}$

3 ND280

ND280 is the near-detector used to constrain many model systematics in the T2K oscillation analysis. It is noticeably different to the far-detector—Super-Kamiokande—in design, geometry, reconstruction and selections, so separate acceptance maps were made for the detectors.

This section briefly goes through the Monte-Carlo and software used in the analysis, the definition of acceptance used for the studies, and the selections and binning. It finishes off with the detector acceptances and documentation of the code.

3.1 Monte-Carlo

Recently processed run 2-8 ND280 Monte-Carlo, provided by the NuMu group, was used for the study. They are available on iRODS at `/QMULZone1/home/asg/asg2018oa/NuMu/MC`. The NEUT version was 5.3.2. The total number of Monte-Carlo events that had a true selection in ND280 was 3,372,569 and 1,615,477 were selected in the ND280 selections. Details can be found in subsection 3.7.

3.2 Selections

The psyche package was used to make the event selections[1]. The multi-π selections for FHC and RHC running were used since they represent T2K BANFF and MaCh3 ND280 analyses at its current state. The 4-π selection (including high and backward going tracks) was not finalised at the time so was not used.

The selections find the highest momentum correctly charged track and identifies it as the lepton candidate. It counts the number of charged pions associated with the vertex and classifies the selection based on that: CC0π, CC1π and CC-other[2]. The presence of any π^0s places an event into the CC-other selection. The selections are further divided by target FGD and FHC and RHC running. In RHC the selections are further split into $\bar{\nu}_\mu$ and ν_μ. The selections are:

- FGD1/2 CC0π FHC
- FGD1/2 CC1π FHC

[1]The specifics of the code and versions are detailed in subsection 3.7

[2]Topology meaning visible topology in the detector. No attempt is made to correct for nuclear effects, such as pion final state interactions, to go back to the primary interaction vertex.

- FGD1/2 CC-other FHC
- FGD1/2 CC0π $\bar{\nu}_\mu$ RHC
- FGD1/2 CC1π $\bar{\nu}_\mu$ RHC
- FGD1/2 CC-other $\bar{\nu}_\mu$ RHC
- FGD1/2 CC0π ν_μ RHC
- FGD1/2 CC1π ν_μ RHC
- FGD1/2 CC-other ν_μ RHC

rendering 18 ND280 selections in total.

3.3 Acceptance

Using aforementioned Monte-Carlo, binning and selection, we proceed by selecting events by their true topology and looking at their reconstructed topology. The event distributions are projected onto particle or interaction kinematics and ratios are formed to give the probability of an event with given true topology to be reconstructed as another topology. The analysis proceeds by:

- Take an ND280 MC event (looking at a `psyche` event's `TrueVertex`es).
- Find the true topology by counting the number of particles with various PDG codes in truth (e.g. $1\mu^-, 2\pi^+, 0\pi^0$) and tag the event as such
- Find the reconstructed ND280 selection given by `psyche`
- Fill a histogram in event some variable (e.g. p_{Lep}) with `True ND280 selection = x` and `Reco ND280 selection = y`: these are events that pass `ND280 selection x` in truth and `ND280 selection y` in reco (x can be equal to y), projected onto p_{Lep}
- Fill a separate histogram in the same variable with `True ND280 selection = x`: this is the normalisation histogram containing all events with `ND280 selection x` in truth
- Divide the first histogram by the second: this gives the probability of an event with `True ND280 selection x` in truth to be reconstructed as `ND280 selection y` in the given variable

Or mathematically,

$$\text{Acceptance of event with } \texttt{True Selection x} \text{ for } \texttt{Reco Selection y} = \frac{\texttt{True Selection x \&\& Reco Selection y}}{\texttt{True Selection x}} \tag{2}$$

which allows us to use a raw event directly from a generator, classify its topology in truth, and look at the probability of it falling into various selections at ND280 after reconstruction.

3.4 Acceptance maps

We now show the acceptances for different projections of the event and different ND280 selections. Herein we only show CC0π and CC1π selections in FHC, although the acceptance maps exist for all selections and all histograms have to be applied on analysis time at the workshop.

Since there are 18 selections and we also include maps for events that don't pass any selections and events that pass any selections, we have 20 maps for each selection. In total this makes 400 maps for a given kinematic variable. We chose six 2D representations of events, so the total number of maps is 2400. However, the probability of an FGD1 event being reconstructed as an FGD2 event is very small, as is the probability of a ν_μ event being reconstructed as $\bar{\nu}_\mu$, so in reality there are much fewer maps that have significant probability.

The plots use the `psyche` ND280 selections enumeration, given for reference in Appendix A.

3.4.1 $p_\mu, \cos\theta_{\nu\mu}$

Figure 3 shows the distributions of events that enter the selection in truth and reco, alongside events that enter the selection in truth. The acceptance of ND280 is then defined as the ratio of the two, shown on the right. We see a familiar efficiency in the 2D map: poor high-angle and backward efficiency with a turn-on at about $\cos\theta_{\nu,\mu} = 0.3, 0.6, 0.8$, reaching about 90% for forward-going tracks above $p_{lep} = 200$ MeV/c.

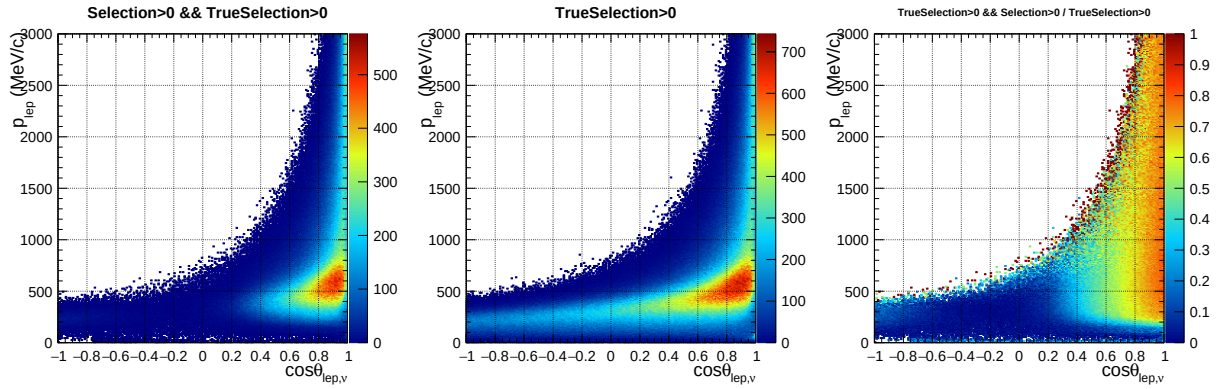

(a) Events which pass any ND280 selection in truth and reco

(b) Events which pass any ND280 selection in truth

(c) Fraction of events which pass any ND280 selection in truth and any ND280 selection in reco to events which pass any ND280 selection in truth

Figure 3: Acceptance map for any true ND280 selection to be reconstructed as any ND280 selection in $(p_\mu, \cos\theta_{\nu\mu})$

Figure 4 shows the acceptances for a true FGD1 CC0π event to fall into any selection, the FGD1 CC0π selection, and the FGD1 CC1π selection. A true FGD1 CC0π event is most likely to fall into the correct selection (followed by no selection at all, when the muon is high-angle or backwards), and very few events enter higher pion multiplicity selections. Generally, the CC0π acceptance map mirrors that of the CC-inclusive selection.

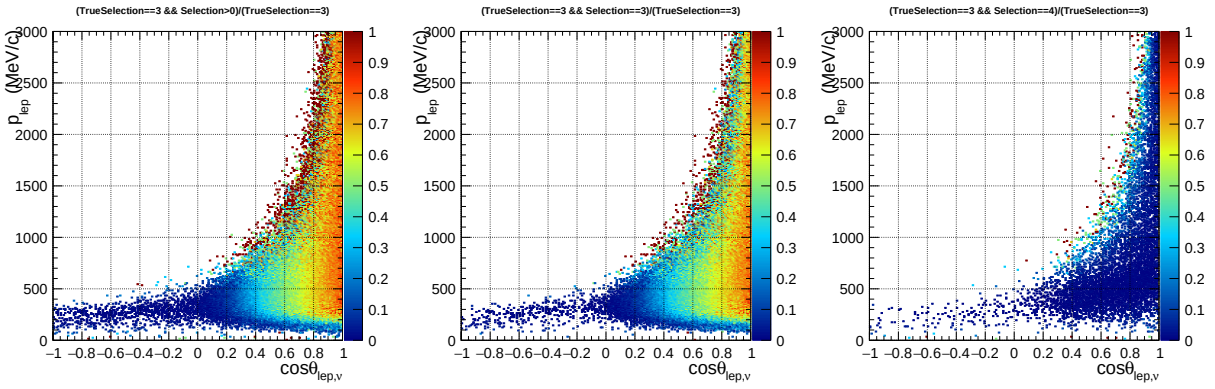

(a) Ratio of events which pass FGD1 CC0π selection in truth and any ND280 selection in reco to events which pass FGD1 CC0π selection in truth

(b) Ratio of events which pass FGD1 CC0π selection in truth and FGD1 CC0π selection in reco to events which pass FGD1 CC0π selection in truth

(c) Ratio of events which pass FGD1 CC0π selection in truth and FGD1 CC1π selection in reco to events which pass FGD1 CC0π selection in truth

Figure 4: Acceptance maps for true FGD1 CC0π events to be reconstructed as different ND280 selections in $(p_\mu, \cos\theta_{\nu\mu})$

Figure 5 shows the equivalent acceptance for CC0π events but in FGD2. The main difference to FGD1 CC0π in Figure 4 is the improved backward reconstruction in FGD2. Very backwards-going tracks reach efficiencies of 20-30%—similar to the efficiency in $\cos\theta_{\nu,\mu} = 0.3 - 0.6$. Otherwise the two detectors are largely similar.

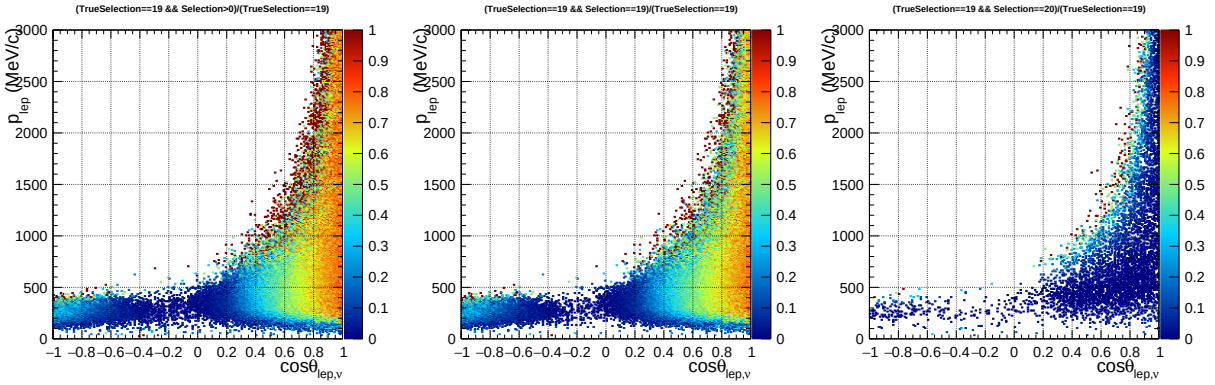

(a) Ratio of events which pass FGD2 CC0π selection in truth and any ND280 selection in reco to events which pass FGD2 CC0π selection in truth

(b) Ratio of events which pass FGD2 CC0π selection in truth and FGD2 CC0π selection in reco to events which pass FGD2 CC0π selection in truth

(c) Ratio of events which pass FGD2 CC0π selection in truth and FGD2 CC1π selection in reco to events which pass FGD2 CC0π selection in truth

Figure 5: Acceptance maps for true FGD2 CC0π events to be reconstructed as different ND280 selections in $(p_\mu, \cos\theta_{\nu\mu})$

3.4.2 $p_\pi, \cos\theta_{\nu\pi}$

Figure 6 looks at the pion kinematics for events that contain pions and enter the selection in truth and reco, and in truth. The main shape of the distribution is captured well by the reconstruction and the acceptance

is largely flat at 0.5-0.6. There is a region of lower acceptance between $p_\pi = 100 - 200$ MeV/c, increasing linearly with $\cos\theta_{\pi,\nu}$ between 0.6-1.0.

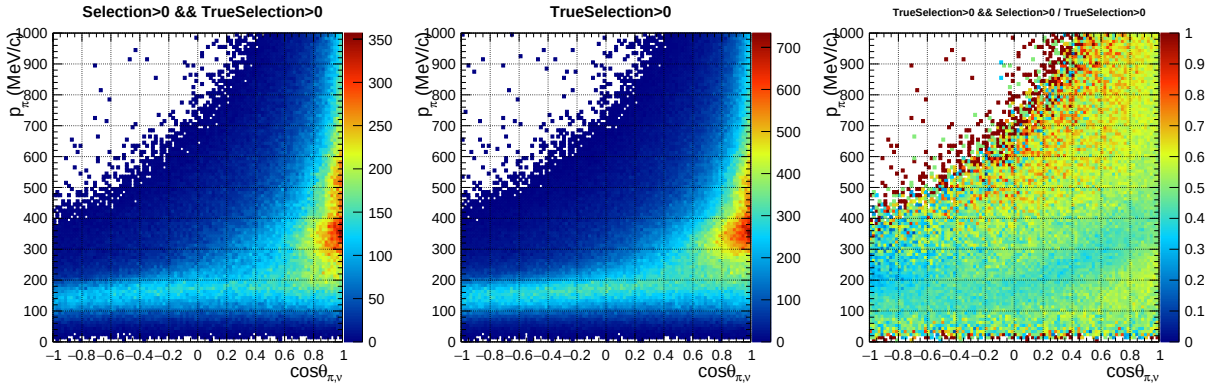

(a) Events passing any ND280 selection in truth and any ND280 selection in reco

(b) Events which pass any ND280 selection in truth

(c) Ratio of event passing any ND280 selection in truth and any ND280 selection in reco to the events passing any ND280 selection in truth.

Figure 6: Acceptance for CC events for all ND280 selections in $(p_\pi, \cos\theta_{\nu\pi})$

Figure 7 shows the distributions for true FGD1 CC1π events. The event distributions are generally in the forward region, with a isotropic angular distribution when $p_\pi = 100-200$ MeV/c. Looking at the true FGD1 CC1π events that are classified as FGD1 CC0π, these events generally don't have forward-going pions and are more likely to have high-angle pions. The FGD1 CC1π events that are correctly classified are generally forward-going and $p_\pi = 200 - 400$ MeV/c although there's an isotropic distribution at 100-200 MeV/c. The acceptances for the true FGD1 CC1π events are shown in the bottom panel. There is a higher probability to classify the event correctly in the very forwards direction, increasing with pion momentum. The probability to incorrectly classify as FGD1 CC0π is highest at high-angles and $p_\pi > 300$ MeV/c.

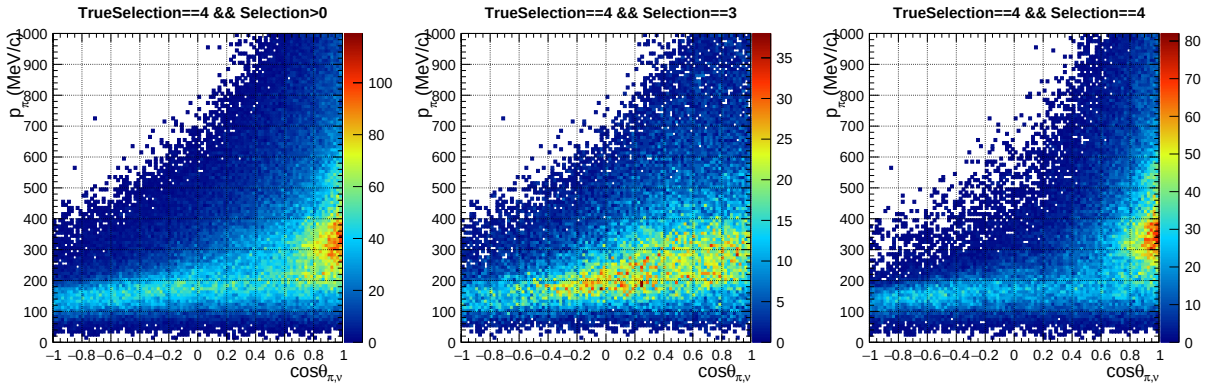

(a) Events passing FGD1 CC1π selection in truth and any ND280 selection in reco

(b) Events passing FGD1 CC1π selection in truth and FGD1 CC0π selection in reco

(c) Events passing FGD1 CC1π selection in truth and FGD1 CC1π selection in reco

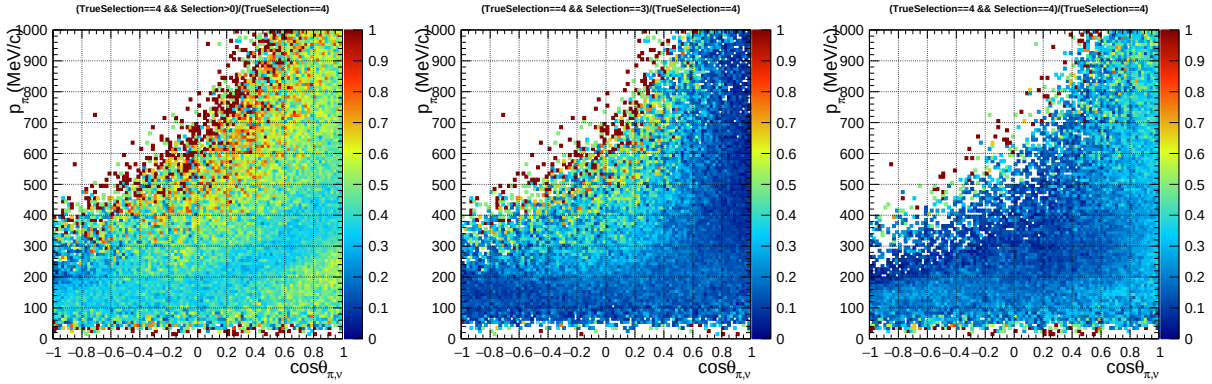

(d) Ratio of events passing FGD1 CC1π in truth and any ND280 selection in reco to events passing FGD1 CC1π in truth

(e) Ratio of events passing FGD1 CC1π in truth and FGD1 CC0π in reco to events passing FGD1 CC1π in truth

(f) Ratio of events passing FGD1 CC1π in truth and FGD1 CC1π in reco to events passing FGD1 CC1π in truth

Figure 7: Acceptances for true FGD1 CC1π events in $(p_\pi, \cos\theta_{\nu\pi})$

3.4.3 $p_\pi, \cos\theta_{\mu,\pi}$

Figure 8 shows the event distributions and acceptances for events with pions in truth, and projects it onto $p_\pi, \cos\theta_{\mu,\pi}$. ND280 again does an adequate job of capturing the overall shape of the distribution, with a flat efficiency in $\cos\theta_{\mu,\pi}$ of about 0.5. The acceptance drastically increases at higher p_π to 0.8-0.9.

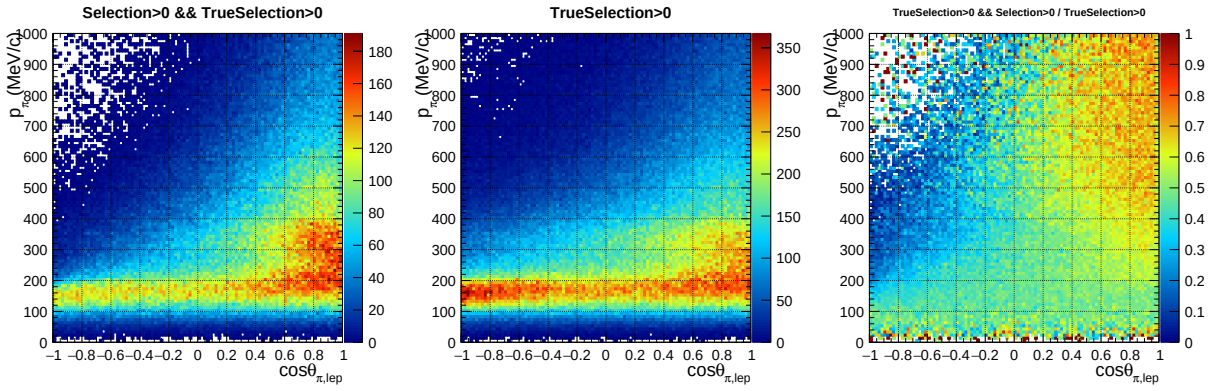

(a) Events which pass any ND280 selection in truth and any ND280 selection in reco

(b) Events which pass any ND280 selection in truth

(c) Ratio of events which pass any ND280 selection in truth and any ND280 selection in reco to events which pass any ND280 selection in truth

Figure 8: Event distributions and acceptance for CC events for all ND280 selections in $(p_\pi, \cos\theta_{\mu,\pi})$

Figure 9 shows the event distributions for events that are true FGD1 CC1π and classified as CC0π, CC1π and CCOther in reconstruction. The events reconstructed as CC0π populate a notably different phase space to CC1π and CCOther: the pion has low momentum (100-300 MeV/c) and largely an isotropic distribution in $\cos\theta_{\pi,\mu}$. The CC1π classified events generally have a higher momentum pion and more collinear μ, π. The events reconstructed as CCOther populate a relatively narrow part of the phase space: $p_\pi = 150-300$ MeV/c and $\cos\theta_{\mu,\pi} > 0.6$.

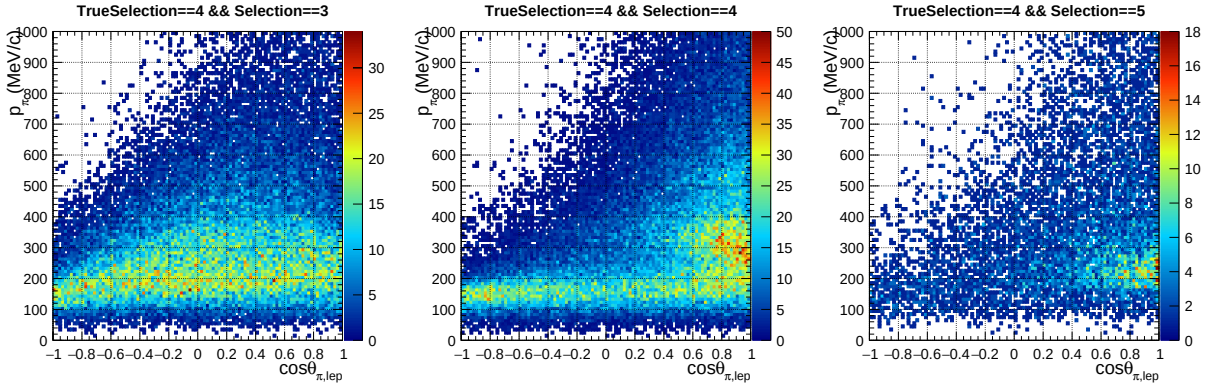

(a) Events which pass FGD1 CC1π selection in truth and FGD1 CC0π in reco

(b) Events which pass FGD1 CC1π selection in truth and FGD1 CC1π in reco

(c) Events which pass FGD1 CC1π selection in truth and FGD1 CCOther in reco

Figure 9: Event distributions for true FGD1 CC1π events reconstructed as CC0π, CC1π and CCOther selections in $(p_\pi, \cos\theta_{\mu,\pi})$

3.4.4 q_0, W_{obs}

Figure 10 shows the q_0, W_{Obs} projection of events, here passing any ND280 selection in truth and reco. The cut around $W_{Obs} = 0.95$ is from CCQE anti-neutrino interactions on Hydrogen. For the acceptance we see clear gradients in the phase space, highest at the maximum W_{Obs} for every q_0 bin (or equivalently in the

lowest q_0 for every W_{Obs} bin).

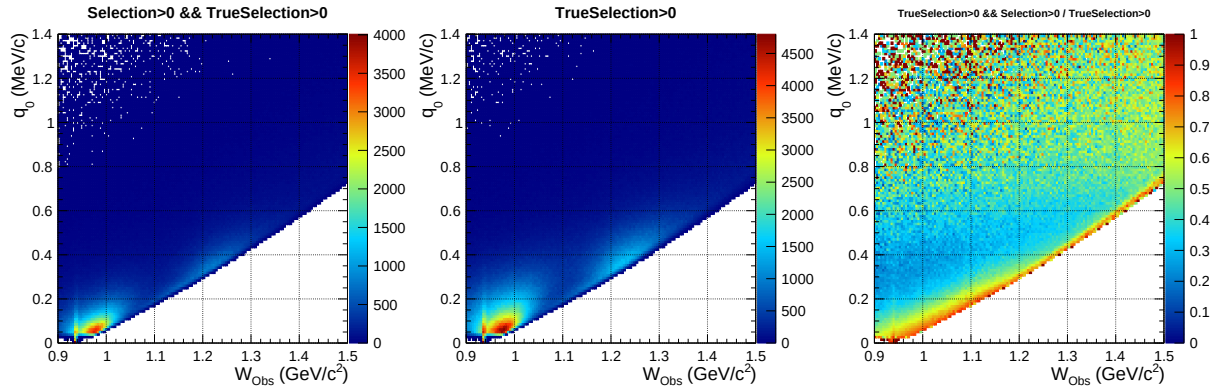

(a) Events passing any ND280 selection in truth and any ND280 selection in reco

(b) Events passing any ND280 selection in truth

(c) Ratio of events passing any ND280 selection in truth and any ND280 selection in reco to events passing any ND280 selection in truth

Figure 10: Acceptance for CC events for all ND280 selections in (q_0, W_{Obs})

Figure 11 shows the acceptances for true FGD1 CC0π events when they are reconstructed in any selection, the correct FGD1 CC0π selection and the incorrect FGD1 CC1π selection. The acceptances are largely similar to the inclusive acceptance.

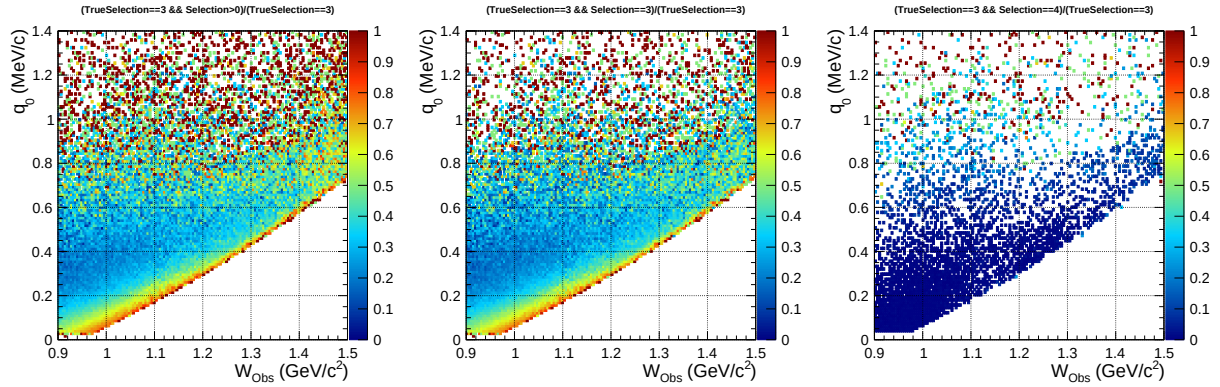

(a) Ratio of events passing FGD1 CC0π selection in truth and any ND280 selection in reco to events passing FGD1 CC0π selection in truth

(b) Ratio of events passing FGD1 CC0π selection in truth and FGD1 CC0π selection in reco to events passing FGD1 CC0π selection in truth

(c) Ratio of events passing FGD1 CC0π selection in truth and FGD1 CC1π selection in reco to events passing FGD1 CC0π selection in truth

Figure 11: Acceptance maps for true FGD1 CC0π events in (q_0, W_{Obs})

Figure 12 shows the acceptances for events with true FGD1 CC1π topology and any reconstructed ND280 topology, FGD1 CC0π topology and FGD1 CC1π topology. Compared to the CC0π acceptances in Figure 11 we see a similar pattern with the highest acceptance being along the highest W_{Obs} in each q_0 bin, and the map starts higher due to the single pion being created at the primary vertex, requiring a higher q_0.

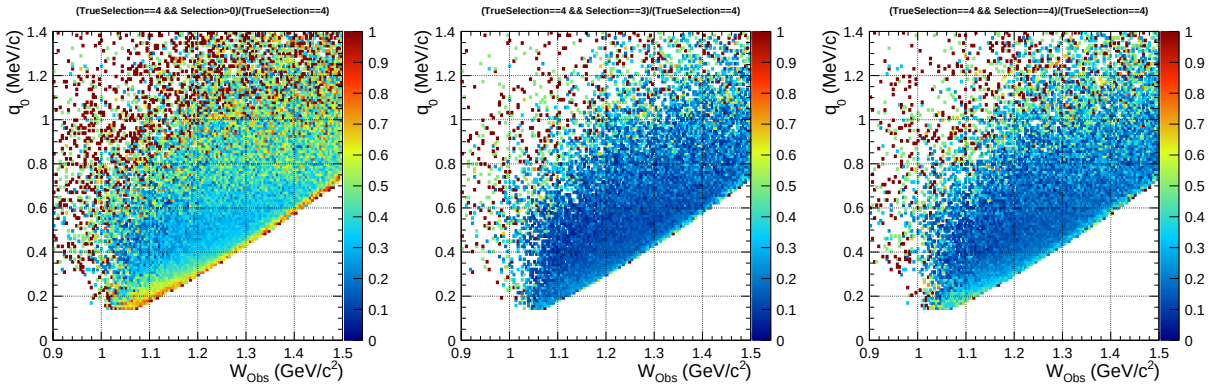

(a) Ratio of events passing FGD1 CC1π selection in truth and any ND280 selection in reco to events passing FGD1 CC1π selection in truth

(b) Ratio of events passing FGD1 CC1π selection in truth and FGD1 CC0π selection in reco to events passing FGD1 CC1π selection in truth

(c) Ratio of events passing FGD1 CC1π selection in truth and FGD1 CC1π selection in reco to events passing FGD1 CC1π selection in truth

Figure 12: Acceptance maps for true FGD1 CC1π events in (q_0, W_{Obs})

3.4.5 q_0, q_3

Figure 13 shows the distribution of events in q_0, q_3 for events that pass any ND280 selection in truth and reco, and the acceptance map. A good portion of the CCQE "lobe" is selected, with excellent acceptance up until $q_0, q_3 = 0.3$ GeV. The acceptance is largely flat in q_0 for a given q_3 bin, except for at the $q_0 = q_3$ edge which has excellent acceptance. Events beyond $q_3 = 0.6$ are barely selected, except for when they have high q_0, which reflects the inability of the current ND280 selections to reconstruct high-angle and backwards tracks.

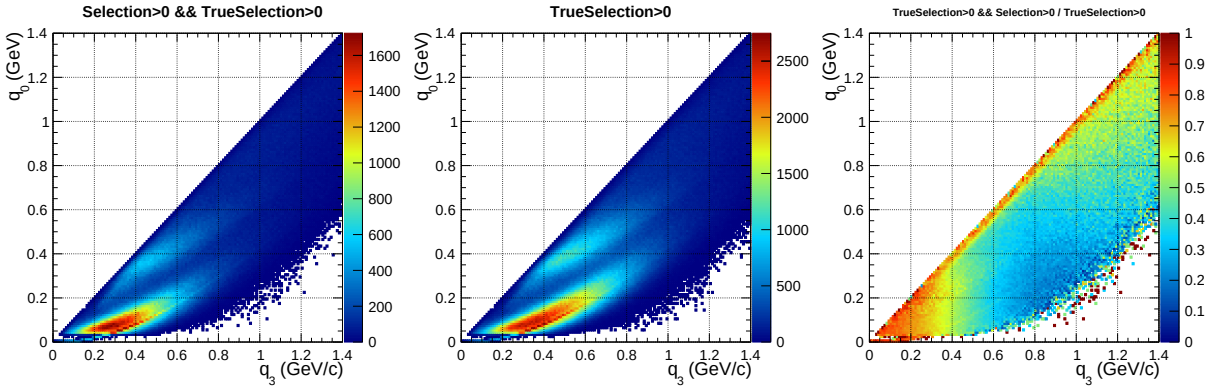

(a) Events passing any ND280 selection in truth and any ND280 selection in reco

(b) Events passing any ND280 selection in truth

(c) Ratio of events passing any ND280 selection in truth and any ND280 selection in reco to events passing any ND280 selection in truth

Figure 13: Acceptance for CC events for all ND280 selections in (q_0, q_3)

Figure 14 shows acceptances for events with true FGD1 CC0π topology. It generally reflects the overall acceptance in Figure 13, with less events at high q_0 as expected.

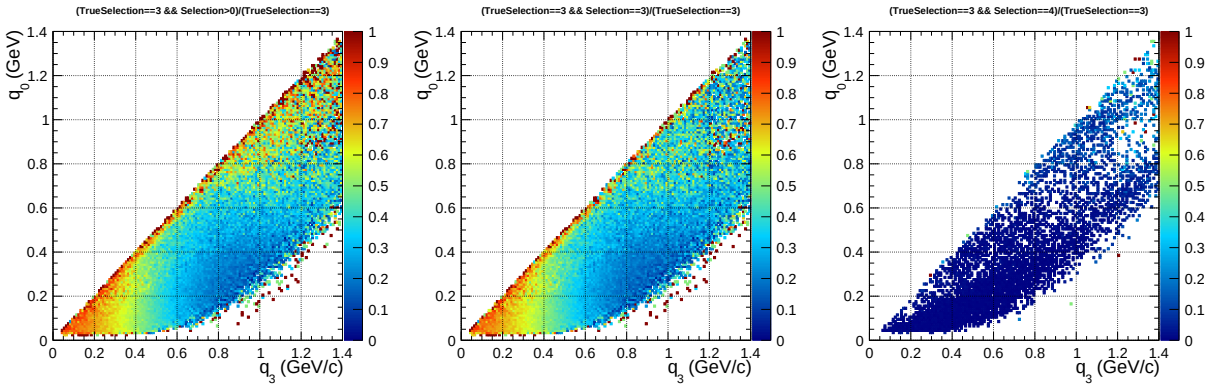

(a) Ratio of events passing FGD1 CC0π selection in truth and any ND280 selection in reco to events passing FGD1 CC0π selection in truth

(b) Ratio of events passing FGD1 CC0π selection in truth and FGD1 CC0π selection in reco to events passing FGD1 CC0π selection in truth

(c) Ratio of events passing FGD1 CC0π selection in truth and FGD1 CC1π selection in reco to events passing FGD1 CC0π selection in truth

Figure 14: Acceptance maps for true FGD1 CC0π events in (q_0, q_3)

Figure 15 shows the acceptances for true FGD1 CC1π events. As for the CC0π selection, the acceptance is good up until $q_0, q_3 = 0.3$ GeV and less so between $q_3 = 0.4 - 1.1$ GeV. The true CC1π events end up being reconstructed in many selections, as is noticeable in the two right-most panels where the acceptances for falling into CC0π and CC1π reconstructions are similar.

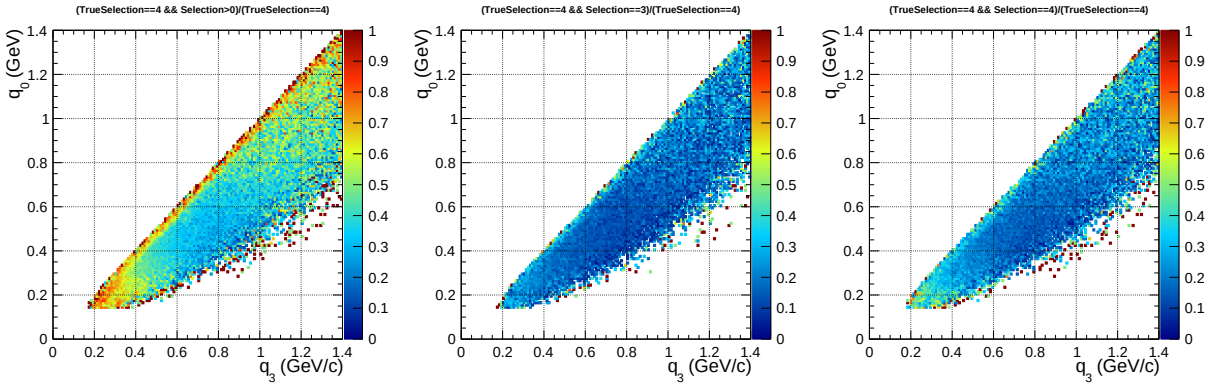

(a) Ratio of events passing FGD1 CC1π selection in truth and any ND280 selection in reco to events passing FGD1 CC1π selection in truth

(b) Ratio of events passing FGD1 CC1π selection in truth and FGD1 CC0π selection in reco to events passing FGD1 CC1π selection in truth

(c) Ratio of events passing FGD1 CC1π selection in truth and FGD1 CC1π selection in reco to events passing FGD1 CC1π selection in truth

Figure 15: Acceptance maps for true FGD1 CC1π events in (q_0, q_3)

3.4.6 E_ν^{True}, y

Figure 16 shows the distribution of events that pass any ND280 selection in reco and truth. Events with $y > 0.2$ are generally poorly reconstructed and are often missed. The acceptance is largely flat at $0.8 in \mathrm{E}_\nu$ for a given y up until $y = 0.15$. The acceptance then shows a wavy pattern and the acceptance has a linear band of about 0.6 acceptance (yellow), below which the acceptance is generally poor (< 0.3).

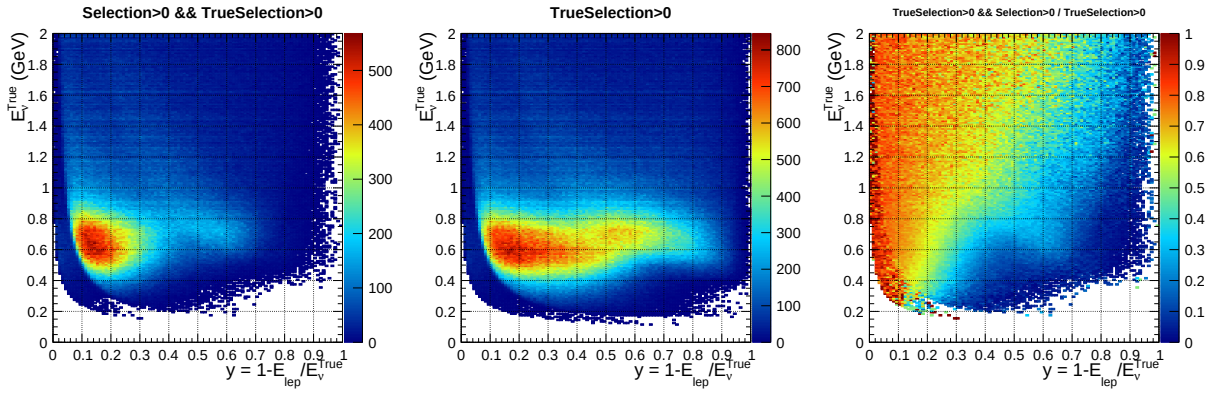

(a) Event distribution for events that pass any ND280 selection in truth and reco

(b) Event distribution for events that pass any ND280 selection in truth

(c) Ratio of events passing any ND280 selection in truth and any ND280 selection in reco to events passing any ND280 selection in truth

Figure 16: Acceptance maps for ND280 CC-inclusive events in E_ν^{True}, y

Figure 18 shows event distributions who's true selection is FGD1 CC0π and falls into any or no ND280 selections. As with Figure 16 many events with $y > 0.2$ are not reconstructed, leading to a CC0π acceptance similar to the CC-inclusive.

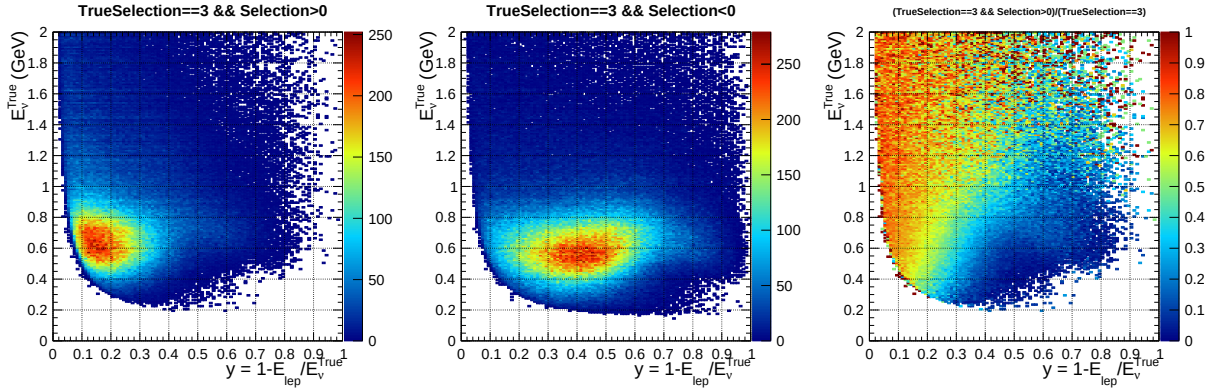

(a) Distribution of events passing FGD1 CC0π in truth and any ND280 selection in reco

(b) Distribution of events passing FGD1 CC0π in truth and no ND280 selection in reco

(c) Ratio of events passing FGD1 CC0π selection in truth and any ND280 selection in reco to events passing FGD1 CC0π selection in truth

Figure 17: Acceptance maps for true FGD1 CC0π events in E_ν^{True}, y

Figure 18 shows the distributions of true FGD1 CC1π events which are reconstructed as any or no ND280 selections. The CC1π events populate a higher $y = 0.4 - 0.7$ than the CC0π events in Figure 18, and the missed events populate an even higher $y > 0.6$. Looking at the acceptance, it is largely flat in E_ν for a given y up until $y = 0.6$.

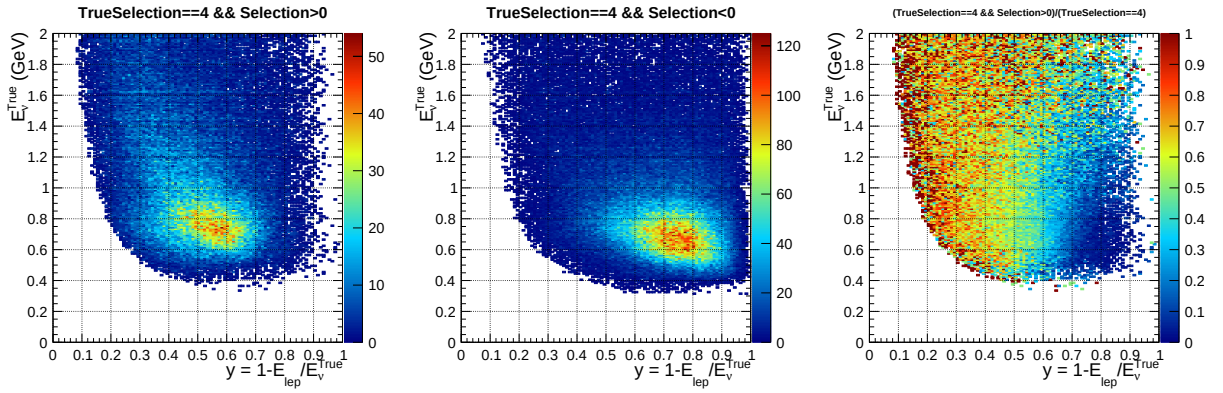

(a) Distribution of events passing FGD1 CC1π selection in truth and any ND280 selection in reco

(b) Distribution of events passing FGD1 CC1π selection in truth and no ND280 selection in reco

(c) Ratio of events passing FGD1 CC1π selection in truth and any ND280 selection in reco to events passing FGD1 CC1π selection in truth

Figure 18: Acceptance maps for true FGD1 CC1π events in (q_0, q_3)

3.5 Detector and particle kinematics resolution

This subsection shows the resolution of ND280 for selected events. They are plotted for CC-inclusive selections, showing lepton and pion kinematics. The particle candidate is selected in `psyche` and its reconstructed and true kinematics are filled. Each bin in the true variable then has a distribution of reconstructed kinematics, and the arithmetic mean and RMS is calculated. There is no check on the true PID of the candidate, meaning a candidate can be any type of true particle (e.g. lepton candidate can be a pion).

3.5.1 Lepton kinematics

Figure 19 shows the smearing for p_{Lep}, where there is largely a linearly increasing resolution (RMS) with p_{Lep}. The best resolution of $\Delta p_{Lep} = 50$ MeV/c is obtained in the 200-300 MeV/c range, which linearly increases with p_{Lep} to 700 MeV/c, where $\Delta p_{Lep} = 70$ MeV/c. The central true value is generally not biased by the reconstruction, except below $p_{Lep} = 100$MeV/c.

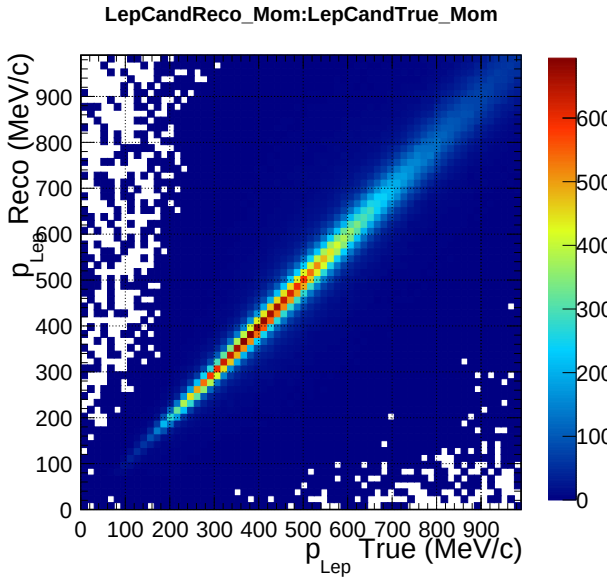

(a) Reco to true mapping for lepton kinematics in p_{Lep}

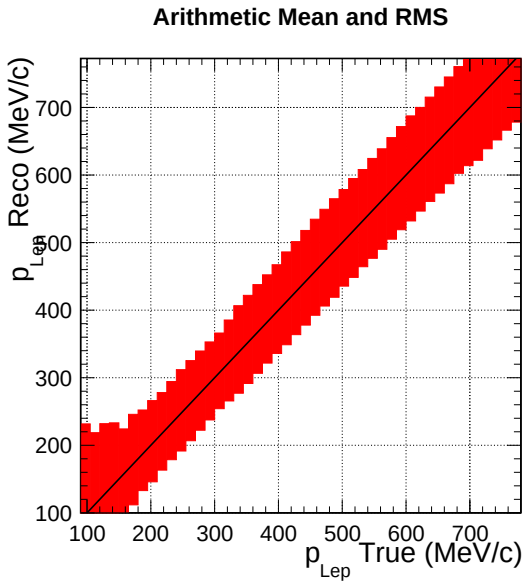

(b) ND280 detector resolution for lepton kinematics in p_{Lep}

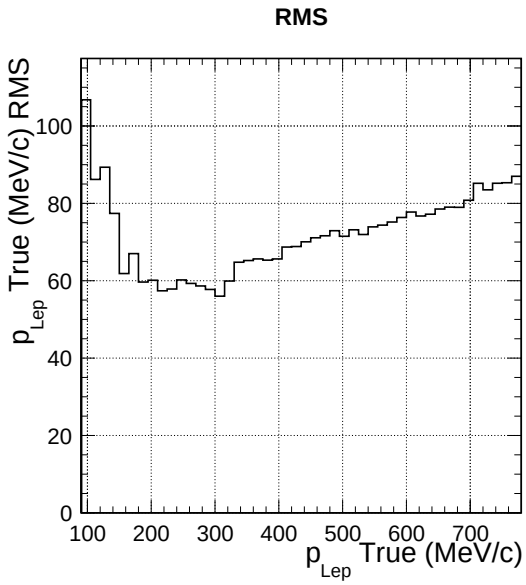

(c) ND280 detector resolution uncertainty in p_{Lep}

Figure 19: ND280 detector characteristics of reconstructing CC-inclusive events in p_{Lep}

Figure 20 shows the equivalent plot projected on to θ_{Lep}. The resolution is 1.5°up until $\theta_{Lep} = 30°$, where it increases linearly to about 3.5°at $\theta_{Lep} = 70°$. The true angle is unbiased by the reconstruction until about 70°. The reconstruction struggles above 80°—both in central value bias and in uncertainty—mostly due to such tracks going along the FGD bars and not leaving hits in the TPC(s). Above 120°there's a decent unbiased reconstruction, albeit with an uncertainty of 20°.

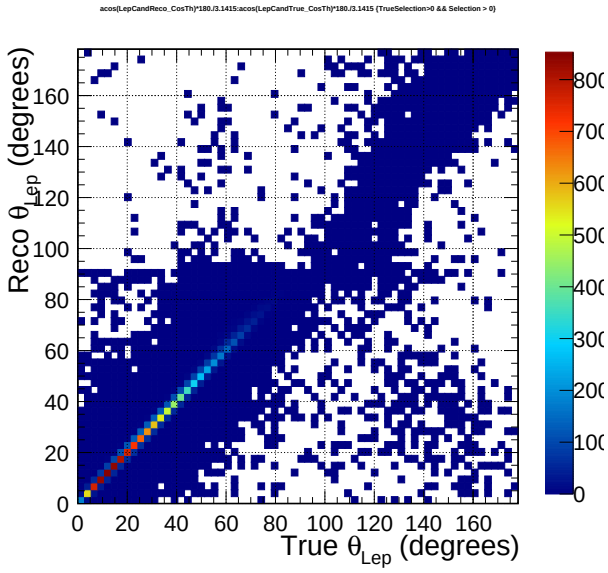

(a) Reco to true mapping for lepton kinematics in θ_{Lep}

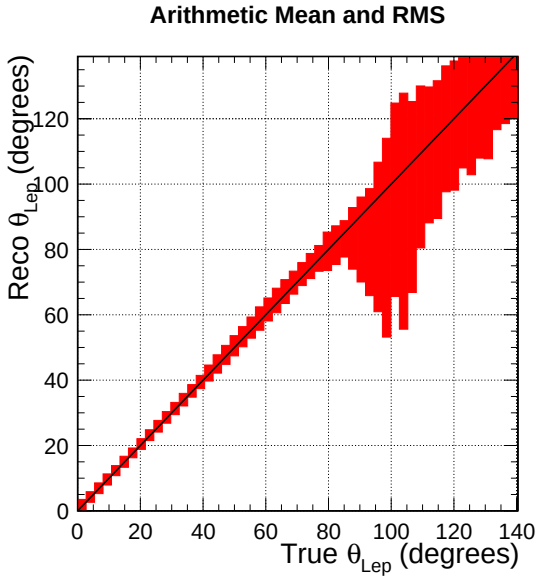

(b) ND280 detector resolution for lepton kinematics in θ_{Lep}

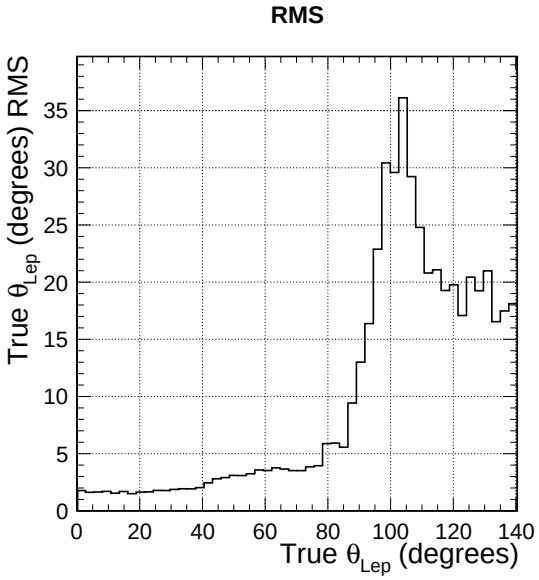

(c) ND280 detector resolution uncertainty in θ_{Lep}

Figure 20: ND280 detector characteristics of reconstructing CC-inclusive events in θ_{Lep}

3.5.2 Pion kinematics

Figure 21 shows the pion momentum resolution for events containing a pion candidate. The central values are unbiased between $p_\pi = 200 - 700$ MeV/c, and are generally bisaed below 150 MeV/c. The resolution on the momentum is similar to the muon case, with the minimum being about 60 MeV/c in the $p_\pi = 200 - 400$ MeV/c range, which linearly increases to about 110 MeV/c at $p_\pi = 700$ MeV/c.

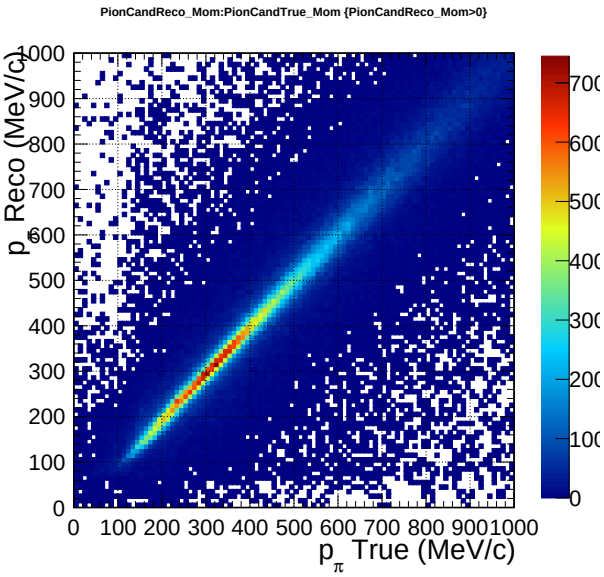

(a) Reco to true mapping for pion kinematics in p_π

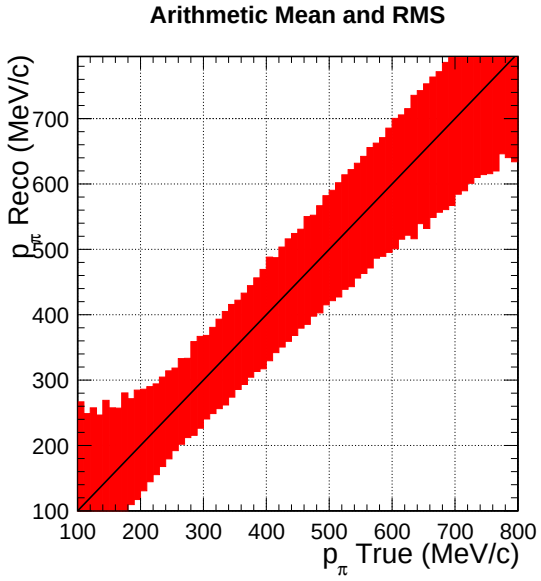

(b) ND280 detector resolution for pion kinematics in p_π

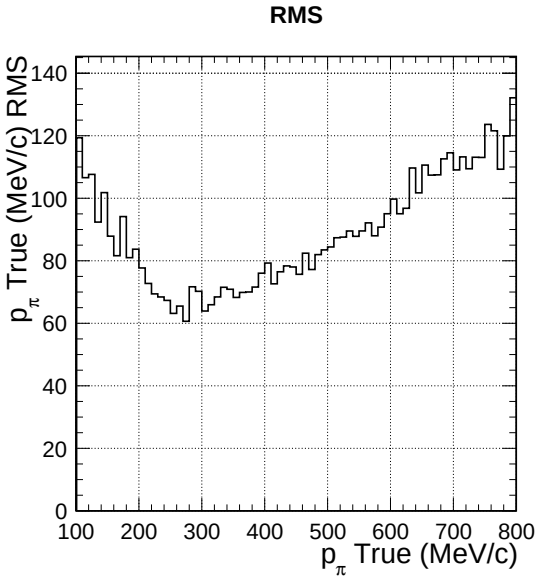

(c) ND280 detector resolution uncertainty in p_π

Figure 21: ND280 detector characteristics of reconstructing CC-inclusive events in p_π

Figure 22 shows the reconstructed pion angle in degrees for a given true pion angle. In the very forward region there is a small bias and a resolution of 4-6°. The resolution is flat at about 5°from $\theta_\pi = 10 - 40°$, after which it linearly increases to 10°at $\theta_\pi = 60°$. As for the muons, the pion reconstruction has the worst resolution in the high-angle and backward region, with uncertainties of 30-50°at $\theta_\pi > 90°$. Above 70°the bias in the central value grows larger and is on-wards unreliable.

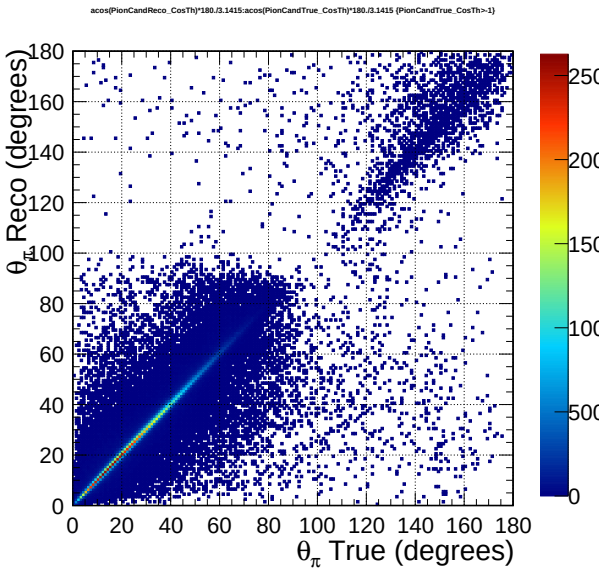

(a) Reco to true mapping for pion kinematics in θ_π

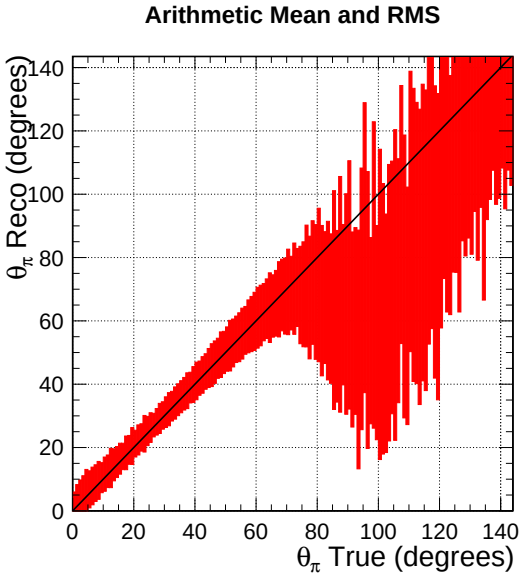

(b) ND280 detector resolution for lepton kinematics in θ_π

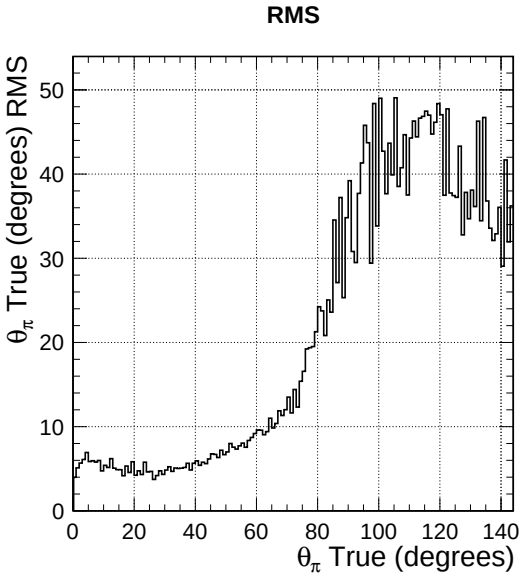

(c) ND280 detector resolution uncertainty in θ_π

Figure 22: ND280 detector characteristics of reconstructing CC-inclusive events in θ_π

3.6 Acceptance under variations of systematics

It was requested to investigate the effects of T2KReWeight cross-section systematics and ND280 detector systematics on the acceptance maps. This was however outside the scope of the studies for the T2K-NOνA workshop, and will be undertaken at a later time.

3.7 Codebase

Code for making ND280 `TTree` using psyche is available at `https://github.com/clarenc3/T2KReWeight/blob/develop/app/MakeAcceptanceMap.cxx`. The NuMu flat-trees are available at `/QMULZone1/home/asg/asg2018oa/NuMu` Code for making the acceptance maps from the `TTree` output is available at `https://github.com/clarenc3/t2k-nova-studies`.

These studies were made with `nd280Highland v2r29` and `nd280Psyche v3r34` (`HEAD` at the time). N.B. The acceptance map code requires the ability to find a `PionCandidate` in an `EventSummaryB`. Check your psyche version carefully: it should be above `v3r33`. A bug was found in the `nd280Psyche` head in which the `PionCandidate` was filled after the `EventSummaryB*` was filled, resulting in `PionCandidate=NULL`.

4 SK

Super-Kamiokande (SK) is the far detector used in the T2K exepriment. It differs from ND280 in many ways including design, reconstruction and selections. This section briefly goes through selections in FHC mode, the true topologies used and the definition of acceptance used. The acceptance maps are then shown for each true definition as well as the maps for when events get mis-reconstructed. Comments on the maps themselves are kept brief, with the hope that they are descriptive enough on their own.

4.1 Monte-Carlo

The Monte-Carlo used for these studies were all FHC mode and included wrong-sign background. The files can be found on iRODS at `/QMULZone1/home/asg/asg2018oa/CC1pidev`. A total of 2,742,275 events were used. No oscillation weights were applied so as to populate the true phase space as much as possible. For similar reason no flux weighting for the MC was used. For clarity the flux of the MC used in these studies are included in figure Figure 23a and with a logarithmic y-scale in figure Figure 23b. A subsequent study of the acceptance with oscillations applied can be done. Furthermore, the same study of RHC mode Monte-Carlo will be performed.

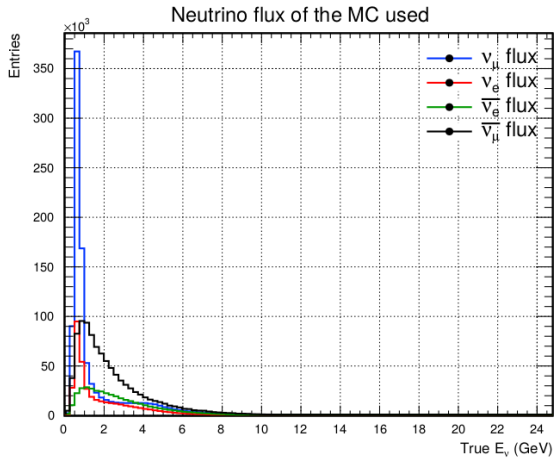

(a)

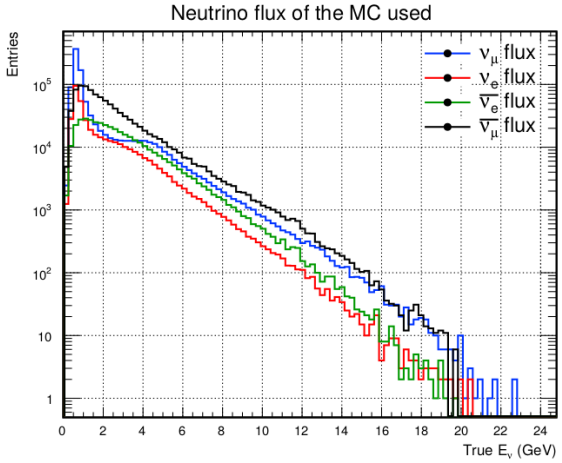

(b)

4.2 Selections and Procedure

The current selections at SK in FHC are comprised of 1Rμ, 1Re and ν_eCC1π^+. Whether a neutrino event makes any given selection (or none at all) is decided by the fiTQun algorithm. More information on the selections and reconstruction at SK can be found in TN-355 (`https://t2k.org/docs/technotes/355`).

This study aims to characterise the different SK selections by looking at truth information. To compare the SK selection and the truth information the true topology at the neutrino interaction vertex has to be found. The process is very similar to that given in section 3.3 except the selection is given by the `iclass` given in the fiTQun output already contained in the MC files. The true topology is then found by looping over the number of particles at the interaction vertex and counting the number of particles with various PDG codes. From this, the true topology can be compared to the selection the event is (or is not) put into. The following truth topologies were defined:

1. **CC**$0\pi 1\mu$—one muon and zero charged or neutral pions are present at the neutrino interaction vertex
2. **CC**$0\pi 1e$—one electron and zero charged or neutral pions are present at the neutrino interaction vertex
3. **CC**$1\pi^+ 1e$—one electron and one (positively) charged pion is present at the neutrino interaction vertex
4. **Other**—any other topology including NC events. This topology is not discussed in these studies further.

These true topologies are used as a signal definition for an SK selection. The CC$0\pi 1e$ is defined as the signal for the 1Re selection. The CC$0\pi 1\mu$ is defined as the signal for the 1Rμ selection. The CC$1\pi^+ 1e$ is defined as the signal for the ν_eCC$1\pi^+$ selection. Furthermore, these topologies are defined inclusively e.g. in the CC$0\pi 1\mu$ topology there could be other final state particles.

Acceptance maps for each SK selection in true phase space have been made for each true topology. In addition, maps showing which areas of phase space lead to mis-identification (mis-ID) of the true topology or which regions result in an event not being selected at all have been made for each true topology. The variables the acceptance and mis-ID maps are made in vary for each sample are given in section 2 and are non-exhaustive. The exact definitions of these variables are given in equation 1. For clarity, the definitions of the z-scale of the acceptance maps for each true topology is given below in equation Equation 3

$$\begin{aligned}
\text{Acceptance}_{\mathbf{CC0\pi 1e}} &= \frac{\text{Truth CC0}\pi 1e \text{ topology \&\& 1R}e \text{ selection}}{\text{Truth CC0}\pi 1e \text{ topology}} \\
\text{Acceptance}_{\mathbf{CC0\pi 1\mu}} &= \frac{\text{Truth CC0}\pi 1\mu \text{ topology \&\& 1R}\mu \text{ selection}}{\text{Truth CC0}\pi 1\mu \text{ topology}} \\
\text{Acceptance}_{\mathbf{CC1\pi^+ 1e}} &= \frac{\text{Truth CC1}\pi^+ 1e \text{ topology \&\& } \nu_e\text{CC1}\pi^+ \text{ selection}}{\text{Truth CC1}\pi^+ 1e \text{ topology}}
\end{aligned} \tag{3}$$

For the mis-ID maps the definitions are slightly different than in Equation 3 with the selection changed to be the "wrong" selection e.g. a CC$0\pi 1e$ event going into the 1Rμ selection. The title of each maps also gives what is being plotted.

4.2.1 CC0π1e acceptance maps

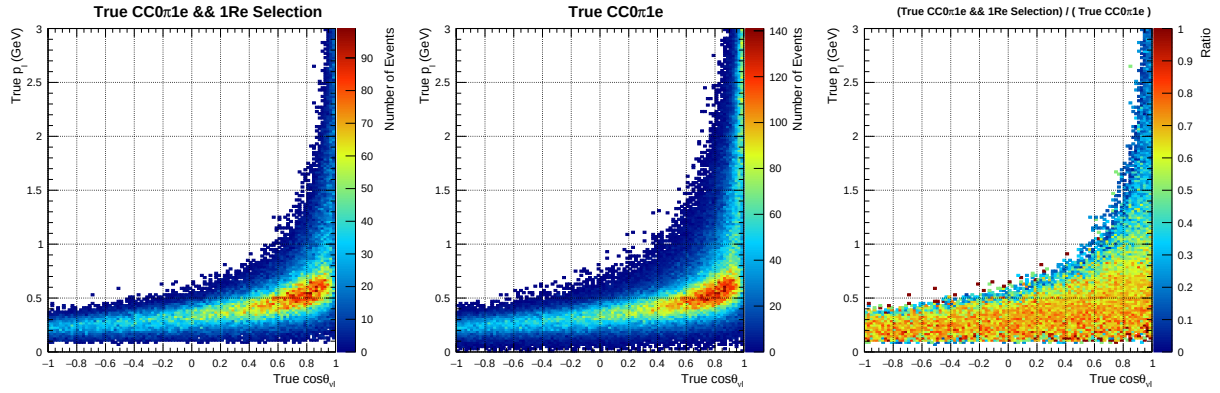

(a) True CC0π1e events passing 1Re selection in p_l and $\cos\theta_{\nu l}$

(b) True CC0π1e events in p_l and $\cos\theta_{\nu l}$

(c) Ratio of true CC0π1e events passing 1Re selection and true CC0π1e events in p_l and $\cos\theta_{\nu l}$

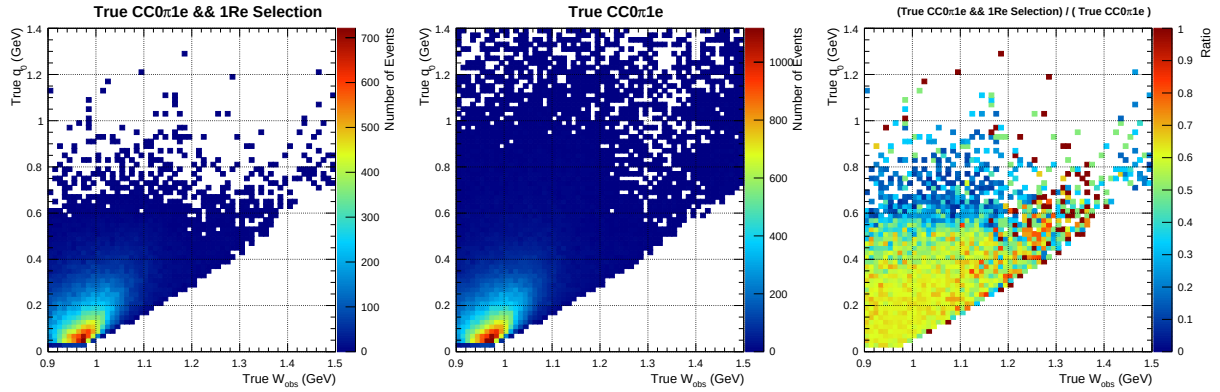

(d) True CC0π1e events passing 1Re selection in q_0 and W_{obs}

(e) True CC0π1e events in q_0 and W_{obs}

(f) Ratio of true CC0π1e events passing 1Re selection and true CC0π1e events in q_0 and W_{obs}

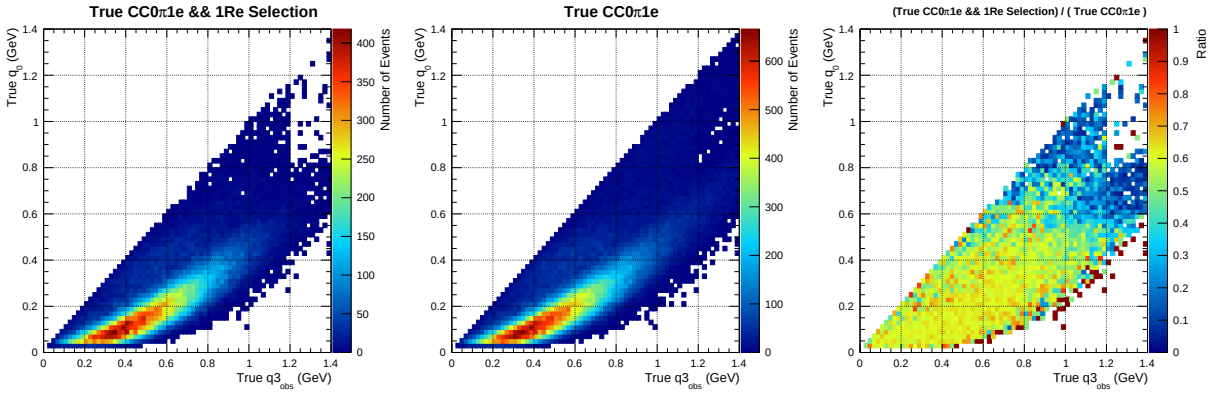

(g) True CC0π1e events passing 1Re selection in q_0 and q_3

(h) True CC0π1e events in q_0 and q_3

(i) Ratio of true CC0π1e events passing 1Re selection and true CC0π1e events in q_0 and q_3

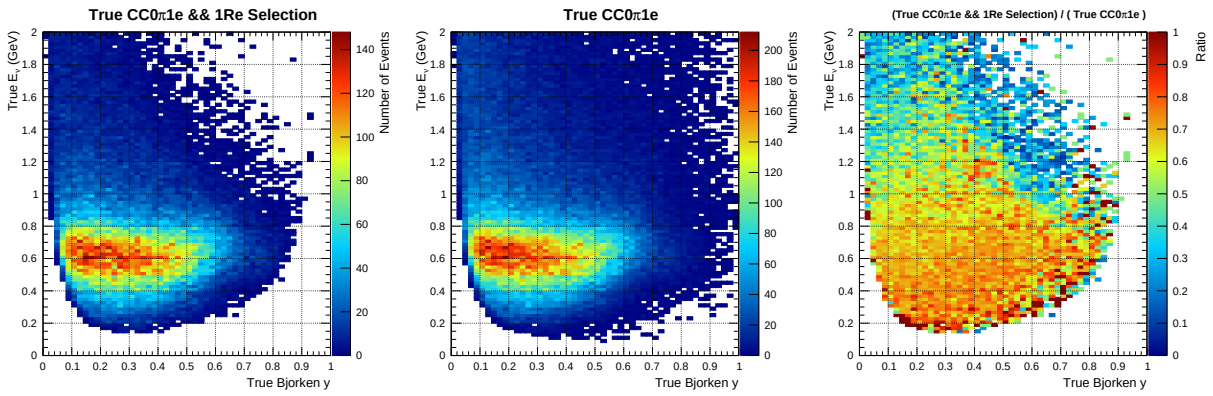

(j) True CC0π1e events passing 1Re selection in E_ν and y

(k) True CC0π1e events in E_ν and y

(l) Ratio of true CC0π1e events passing 1Re selection and true CC0π1e events in E_ν and y

Figure 24: Acceptance maps for true CC0π1e events in (p_l, $\cos\theta_{\nu l}$), (q_0, W_{obs}), (q_0, q_3) and (E_ν, y)

Generally, CC0π1e events have a high efficiency of being selected as 1Re. One can see in 24 c) that the acceptance is fairly flat in $\cos\theta_{\nu l}$ and drops off as p_l approaches 1GeV. In c) the requirement in the selection for the reconstructed electron to have at least 100MeV of energy can be seen. The sharp cut off at 100MeV is a reflection of the good momentum resolution in this region. Figures 24 f) and i) show that the efficiency is highest in the regions where CCQE is expected to dominate.

4.2.2 CC0π1e mis-ID maps

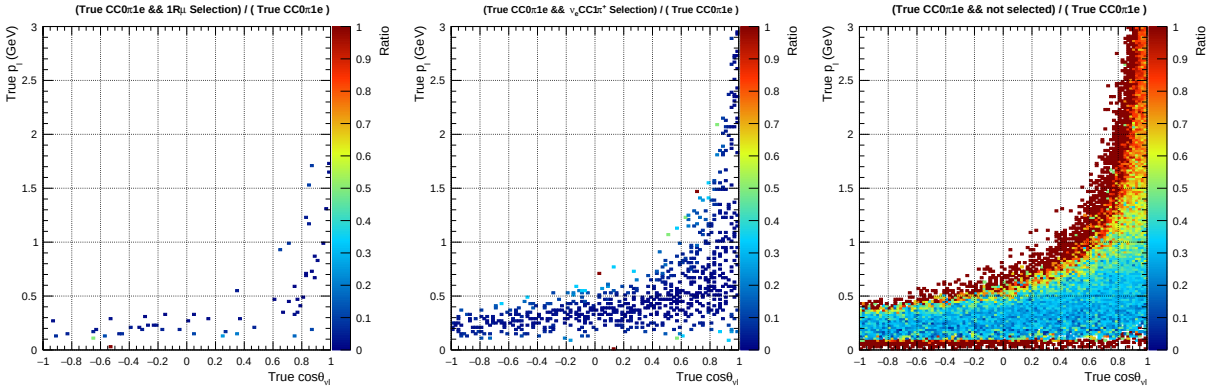

(a) True CC0π1e events passing 1Rμ selection in p_l and $\cos\theta_{\nu l}$

(b) True CC0π1e events passing ν_eCC1π^+1e selection in p_l and $\cos\theta_{\nu l}$

(c) True CC0π1e events passing no selection in p_l and $\cos\theta_{\nu l}$

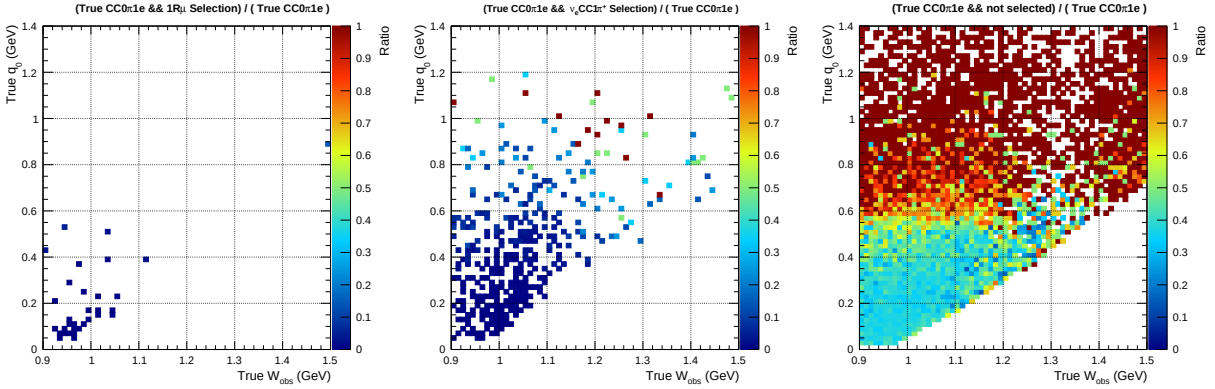

(d) True CC0π1e events passing 1Rμ selection in q_0 and W_{obs}

(e) True CC0π1e events passing ν_eCC1π^+1e selection in q_0 and W_{obs}

(f) True CC0π1e events passing no selection in q_0 and W_{obs}

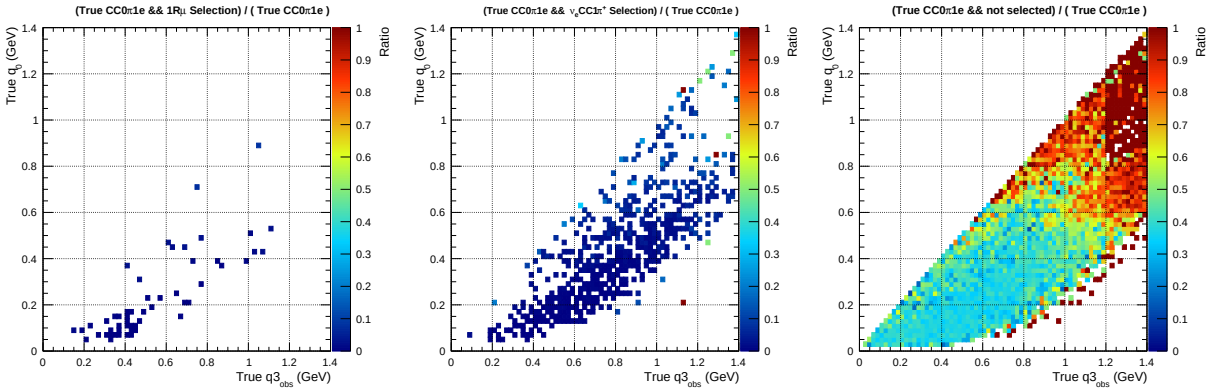

(g) True CC0π1e events passing 1Rμ selection in q_0 and q_3

(h) True CC0π1e events passing ν_eCC1π^+1e selection in q_0 and q_3

(i) True CC0π1e events passing no selection in q_0 and q_3

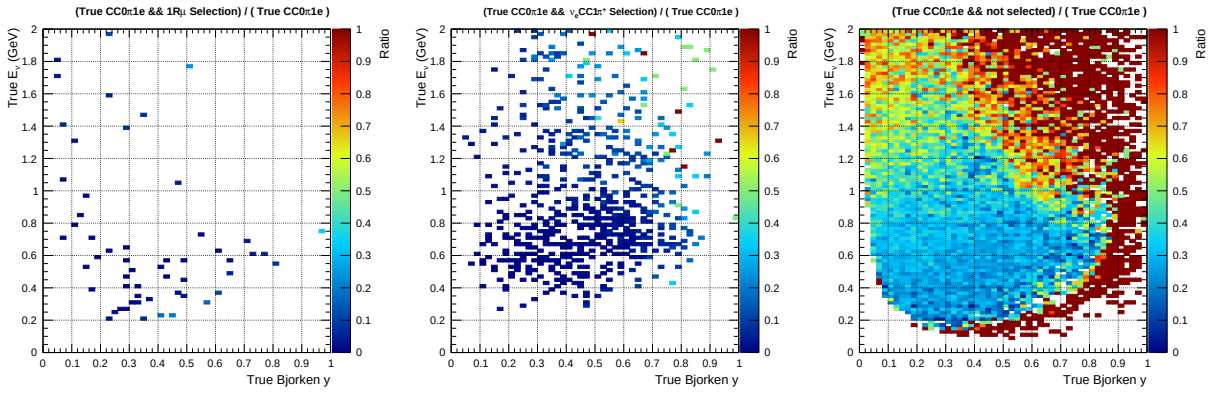

(j) True CC0π1e events passing 1Rμ selection in E_ν and y

(k) True CC0π1e events passing ν_eCC1π^+1e selection in E_ν and y

(l) True CC0π1e events passing no selection in E_ν and y

Figure 25: Mis-ID plots for true CC0π1e events in $(p_l, cos\theta_{\nu l})$, (q_0, W_{obs}), (q_0, q_3), and (E_ν, y)

Figure 25, shows that there is generally a low probability of a true CC0π1e event being selected as 1Rμ or ν_eCC1π^+1e with no clear dependence on any of the variables used. However, for true CC0π1e events which do not pass any selection there are strong dependencies. Most notable are in 25 c) where electrons below the 100MeV reconstruction threshold mostly do not get selected and in 25 f) and i) the probability of not being selected increases for $q_0 > 0.6$GeV. This could be due to the definitions of the CC0π1e topology not having any strict cuts on the number of other particles apart from pions and electrons and for events with high energy transfer the probability of producing more final state particles increases.

4.2.3 CC$0\pi 1\mu$ acceptance maps

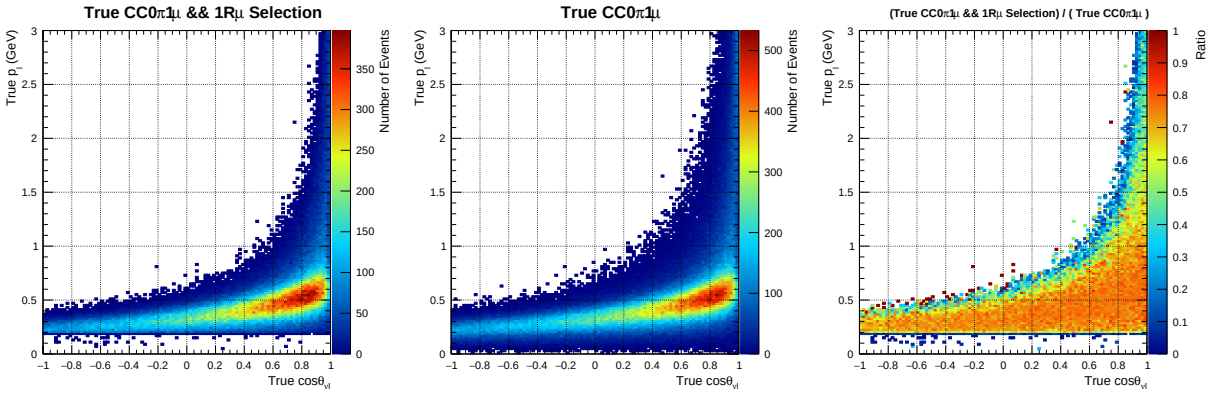

(a) True CC$0\pi 1\mu$ events passing 1Rμ selection in p_l and $\cos\theta_{\nu l}$

(b) True CC$0\pi 1\mu$ events in p_l and $\cos\theta_{\nu l}$

(c) Ratio of true CC$0\pi 1\mu$ events passing 1Rμ selection and true CC$0\pi 1\mu$ events in p_l and $\cos\theta_{\nu l}$

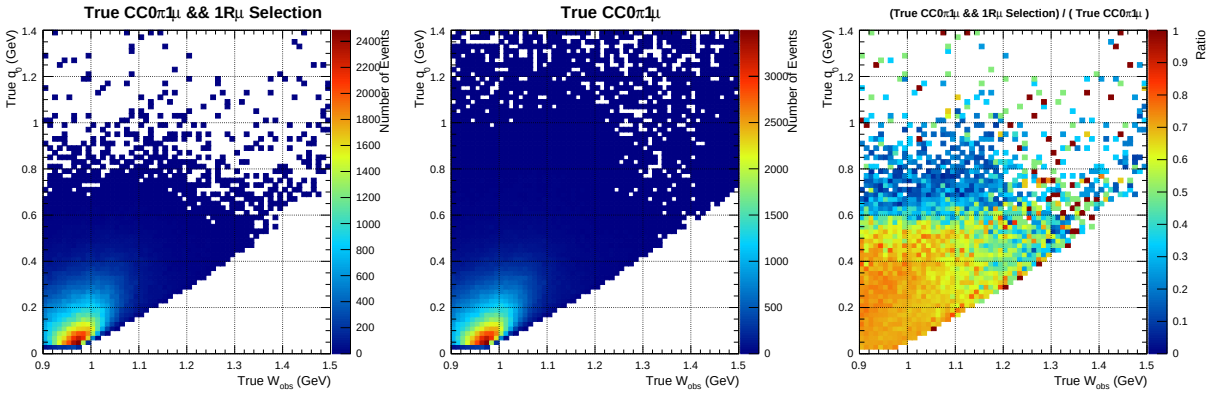

(d) True CC$0\pi 1\mu$ events passing 1Rμ selection in q_0 and W_{obs}

(e) True CC$0\pi 1\mu$ events in q_0 and W_{obs}

(f) Ratio of true CC$0\pi 1\mu$ events passing 1Rμ selection and true CC$0\pi 1\mu$ events in q_0 and W_{obs}

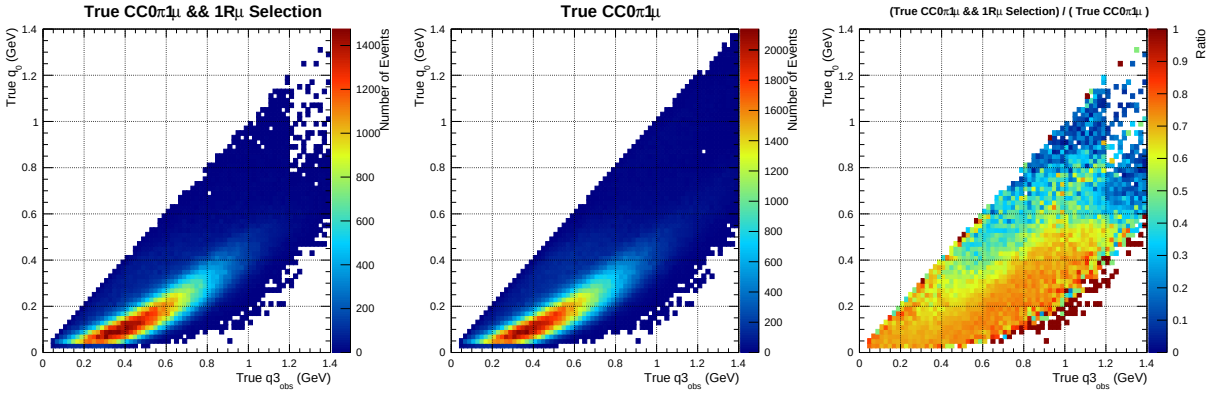

(g) True CC$0\pi 1\mu$ events passing 1Rμ selection in q_0 and q_3

(h) True CC$0\pi 1\mu$ events in q_0 and q_3

(i) Ratio of true CC$0\pi 1\mu$ events passing 1Rμ selection and true CC$0\pi 1\mu$ events in q_0 and q_3

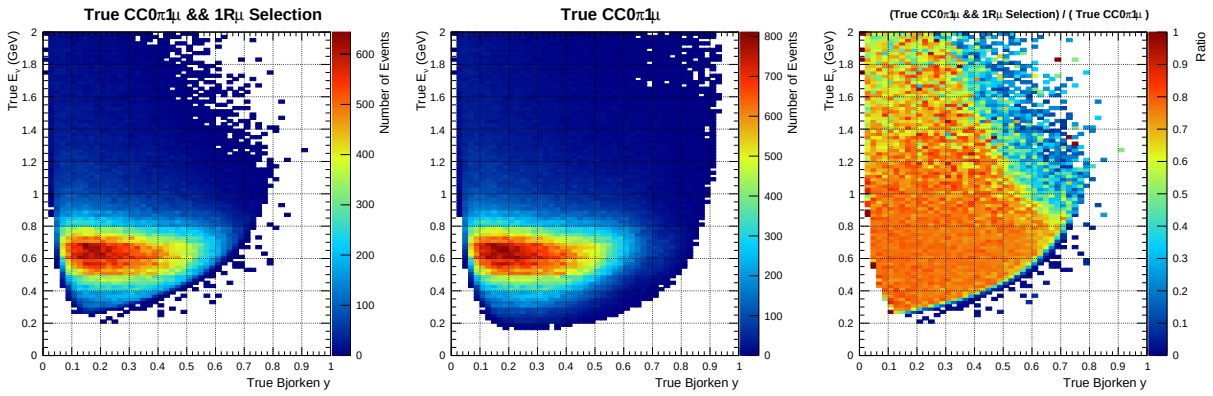

(j) True CC0π1μ events passing 1Rμ selection in E_ν and y

(k) True CC0π1μ events in E_ν and y

(l) Ratio of true CC0π1μ events passing 1Rμ selection and true CC0π1μ events in E_ν and y

Figure 26: Efficiency plots for true CC0π1μ events in (p_l, $\cos\theta_{\nu l}$), (q_0, W_{obs}), (q_0, q_3) and (E_ν, y)

True CC0π1μ events have a high efficiency of being selected correctly. Figure 26 c) shows a fairly broad acceptance in $\cos\theta_{\nu l}$ with a drop in efficiency coming at around 2GeV for the most forward going leptons. Again, there is a clear cut off in lepton momentum at 200MeV which is the energy the muon is required to have to make the selection. The fact that this is clear in the true lepton momentum shows that the momentum resolution is good in this region. In figures 26 f) and 26 i) the efficiency again is high in the region where CCQE is expected to be the main interaction.

4.2.4 CC0π1μ mis-ID maps

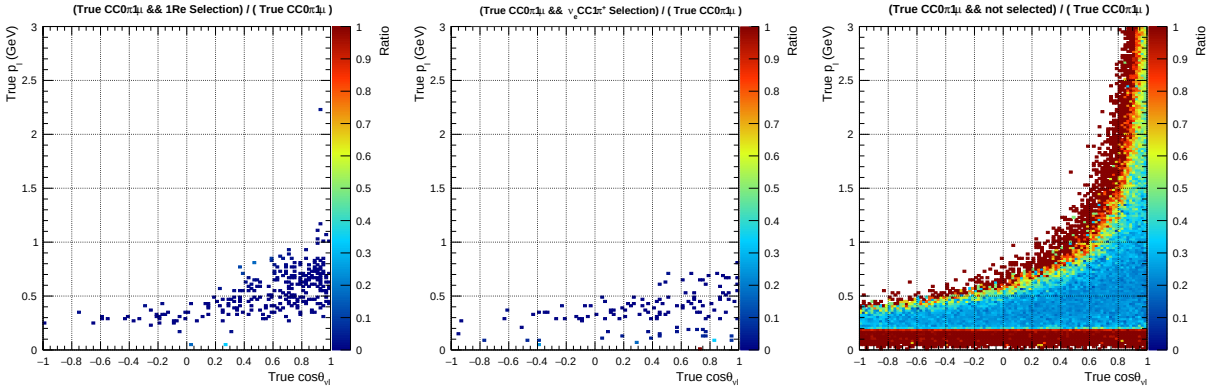

(a) True CC0π1μ events passing 1Re selection in p_l and $\cos\theta_{\nu l}$

(b) True CC0π1μ events passing ν_eCC1π^+1e selection in p_l and $\cos\theta_{\nu l}$

(c) True CC0π1μ events passing no selection in p_l and $\cos\theta_{\nu l}$

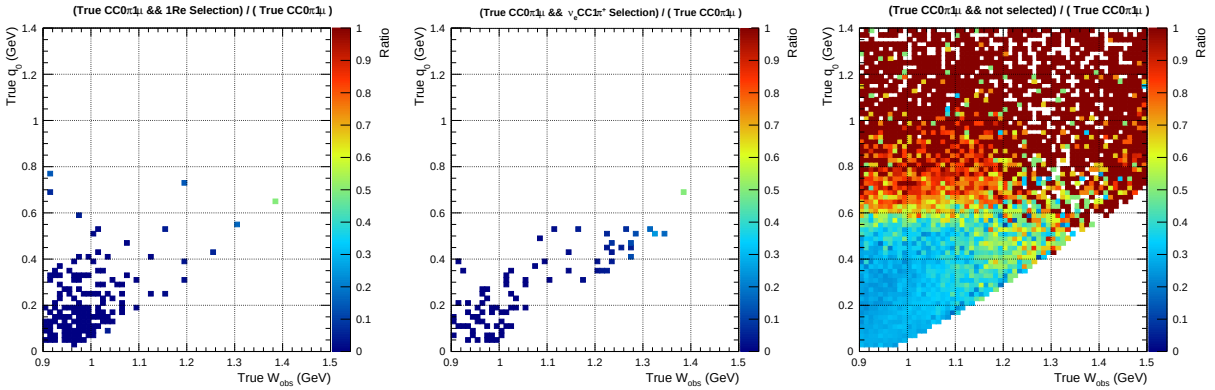

(d) True CC0π1μ events passing 1Re selection in q_0 and W_{obs}

(e) True CC0π1μ events passing ν_eCC1π^+1e selection in q_0 and W_{obs}

(f) True CC0π1μ events passing no selection in q_0 and W_{obs}

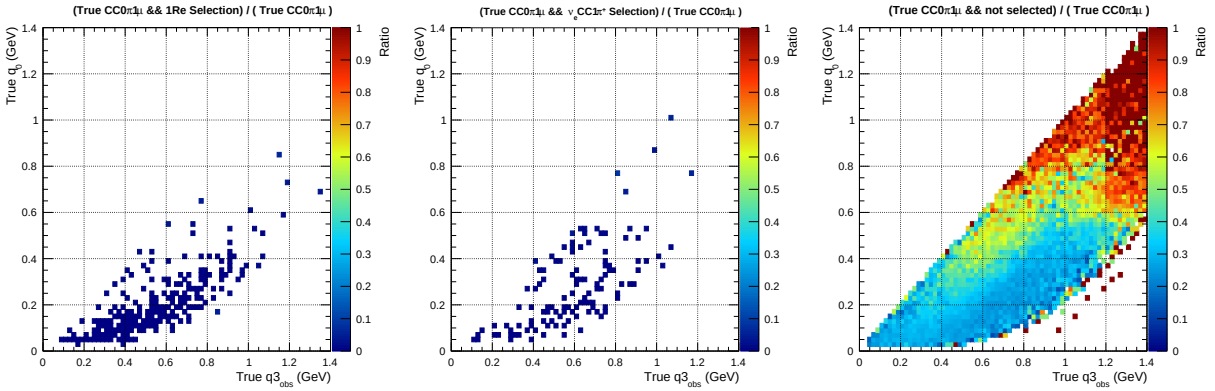

(g) True CC0π1μ events passing 1Re selection in q_0 and q_3

(h) True CC0π1μ events passing ν_eCC1π^+1e selection in q_0 and q_3

(i) True CC0π1μ events passing no selection in q_0 and q_3

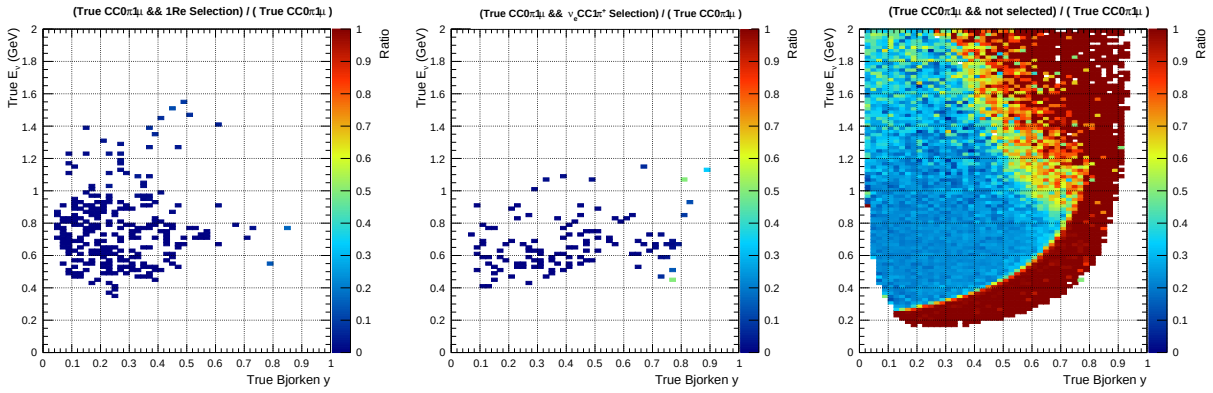

(j) True CC0π1μ events passing 1Re selection in E_ν and y

(k) True CC0π1μ events passing ν_eCC1π^+1e selection in E_ν and y

(l) True CC0π1μ events passing no selection in E_ν and y

Figure 27: Mis-ID plots for true CC0π1μ events in $(p_l, cos\theta_{\nu l})$, (q_0, W_{obs}), (q_0, q_3), and (E_ν, y)

Generally, the mis-ID probability is again low for CC0π1μ with very few events being selected as 1Re or ν_eCC1π^+. However, we see in figure 27 c) that there is a clear point below the 200 GeV where true CC0π1μ events do not get selected. Similar to true CC0π1e there appears to be a significant rise in the probability of true CC0π1μ events not being selected for $q_0 > 0.6$GeV. This could, again, be due to the definitions of the CC0π1μ topology not having any strict cuts on the number of other particles apart from pions and muons.

4.2.5 CC$1\pi^+1e$ efficiency maps

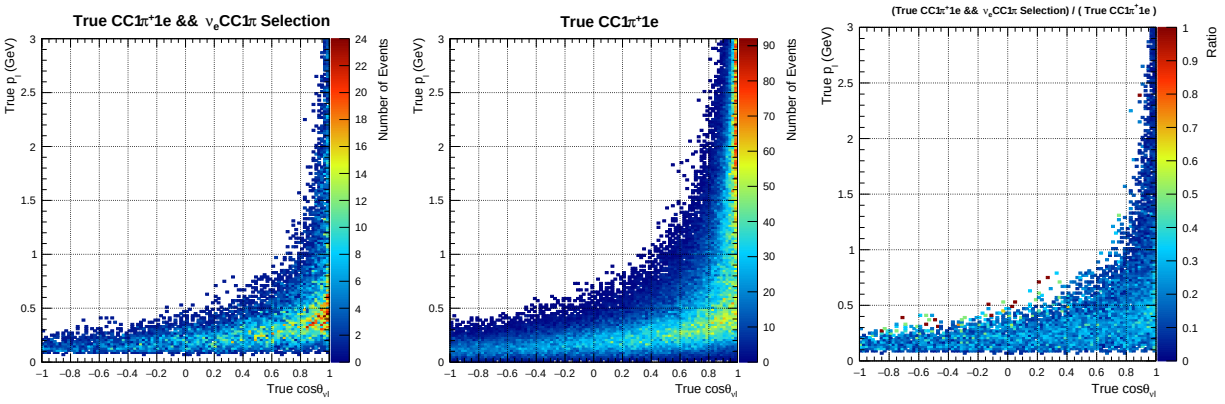

(a) True CC$1\pi^+1e$ events passing ν_eCC$1\pi^+$ selection in p_l and $\cos\theta_{\nu l}$ (b) True CC$1\pi^+1e$ events in p_l and $\cos\theta_{\nu l}$ (c) Ratio of true CC$1\pi^+1e$ events passing ν_eCC$1\pi^+$ selection and true CC$1\pi^+1e$ events in p_l and $\cos\theta_{\nu l}$

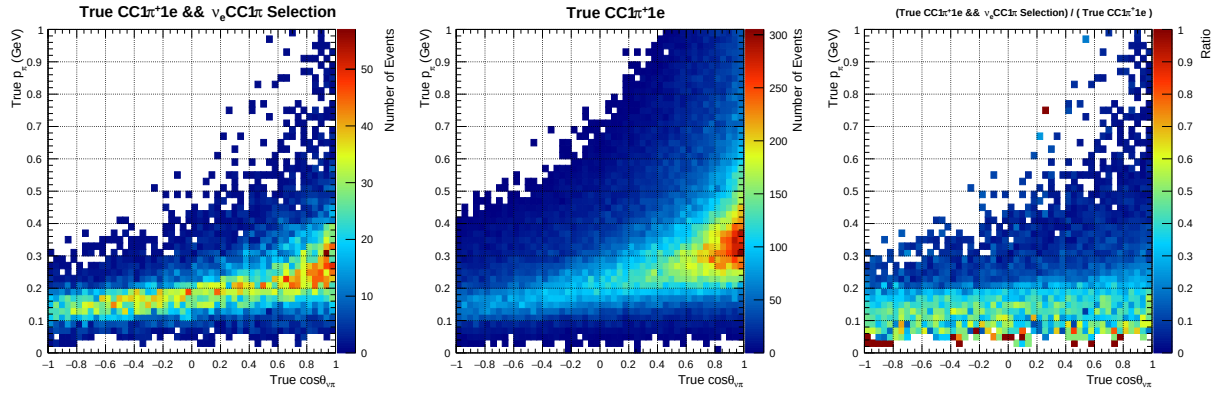

(d) True CC$1\pi^+1e$ events passing ν_eCC$1\pi^+$ selection in p_π and $\cos\theta_{\nu\pi}$ (e) True CC$1\pi^+1e$ events in p_π and $\cos\theta_{\nu\pi}$ (f) Ratio of true CC$1\pi^+1e$ events passing ν_eCC$1\pi^+$ selection and true CC$1\pi^+1e$ events in p_π and $\cos\theta_{\nu\pi}$

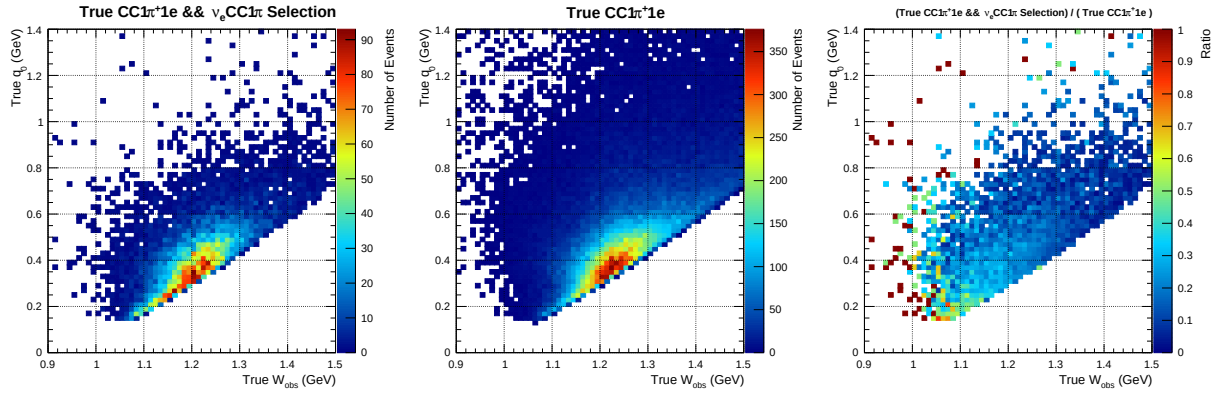

(g) True CC$1\pi^+1e$ events passing ν_eCC$1\pi^+$ selection in q_0 and W_{obs} (h) True CC$1\pi^+1e$ events in q_0 and W_{obs} (i) Ratio of true CC$1\pi^+1e$ events passing ν_eCC$1\pi^+$ selection and true CC$1\pi^+1e$ events in q_0 and W_{obs}

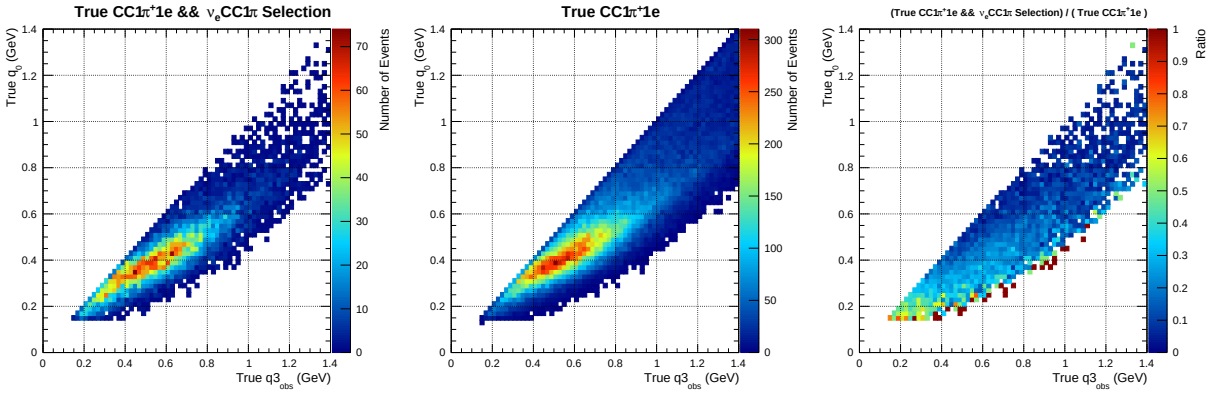

(j) True CC1π^+1e events passing ν_eCC1π^+ selection in q_0 and q_3

(k) True CC1π^+1e events in q_0 and q_3

(l) Ratio of true CC1π^+1e events passing ν_eCC1π^+ selection and true CC1π^+1e events in q_0 and q_3

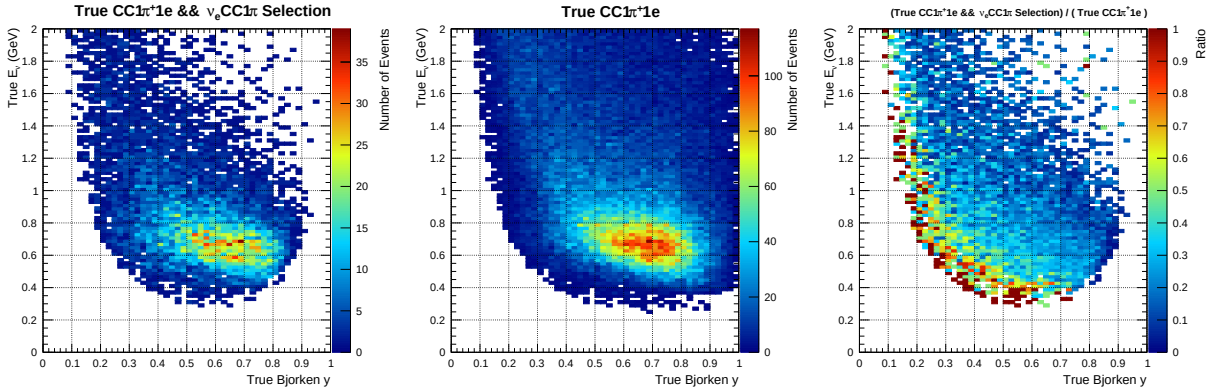

(m) True CC1π^+1e events passing ν_eCC1π^+ selection in E_ν and y

(n) True CC1π^+1e events in E_ν and y

(o) Ratio of true CC1π^+1e events passing ν_eCC1π^+ selection and true CC1π^+1e events in E_ν and y

Figure 28: Acceptance maps for true CC1π^+1e events in (p_l, $\cos\theta_{\nu l}$), (p_π, $\cos\theta_{\nu\pi}$), (q_0, W_{obs}), (q_0, q_3) and (E_ν, y)

The efficiency for CC1π^+1e is generally lower compared to the previous two topologies. The efficiency in lepton momentum and angle is very flat as can be seen in 28 c) except for the 100MeV reconstruction requirement much like the CC0π1e events. However, one can see in 28 f) a clear reduction in efficiency as pion momentum increases. This may be due to pions with higher momenta being more likely to produce Cerenkov radiation and fail the requirement that there is only one ring. The efficiency in 28 i), l) and o) can also be seen to be fairly flat but now across a region where the dominant interaction is expected to be resonant pion production.

4.2.6 CC1π^+1e mis-ID maps

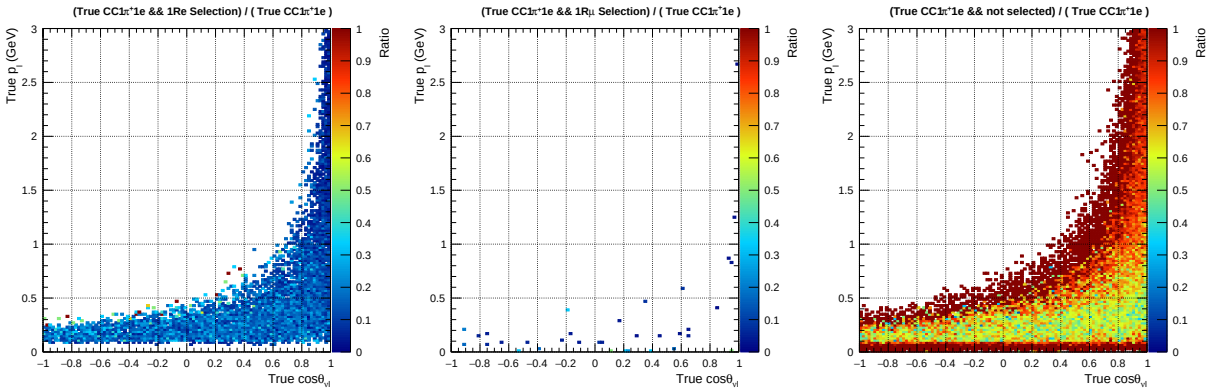

(a) True CC1π^+1e events passing 1Re selection in p_l and $\cos\theta_{\nu l}$

(b) True CC1π^+1e events passing 1Rμ selection in p_l and $\cos\theta_{\nu l}$

(c) True CC1π^+1e events passing no selection in p_l and $\cos\theta_{\nu l}$

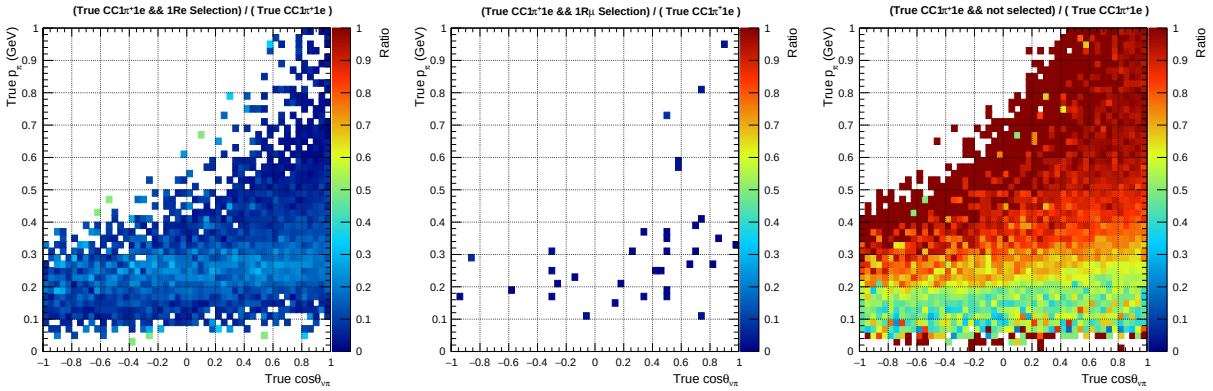

(d) True CC1π^+1e events passing 1Re selection in p_π and $\cos\theta_{\nu\pi}$

(e) True CC1π^+1e events passing 1Rμ selection in p_π and $\cos\theta_{\nu\pi}$

(f) True CC1π^+1e events passing no selection in p_π and $\cos\theta_{\nu\pi}$

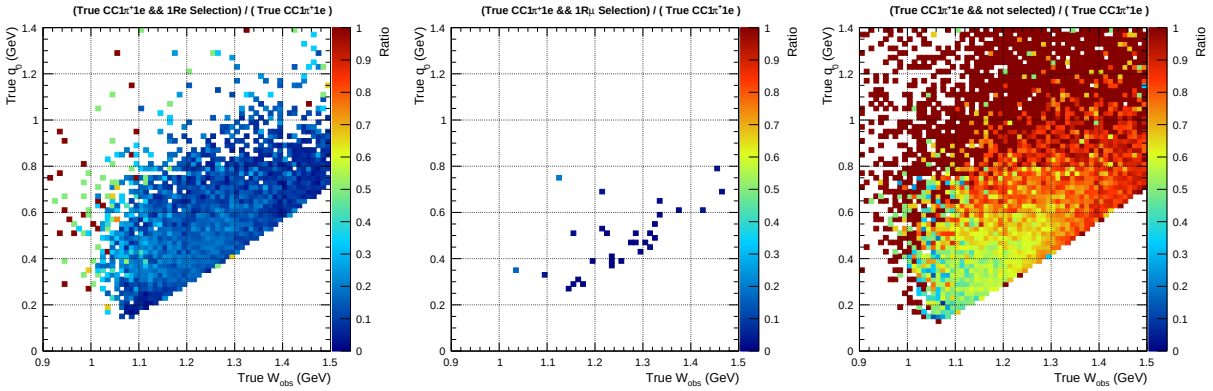

(g) True CC1π^+1e events passing 1Re selection in q_0 and W_{obs}

(h) True CC1π^+1e events passing 1Rμ selection in q_0 and W_{obs}

(i) True CC1π^+1e events passing no selection in q_0 and W_{obs}

True CC1π^+1e events appear to have low but non-negligible probability of being selected as 1Re events. This can be seen in figures 29 a),d),g),j) and m) but this probability appears not to be highly dependent on any of the variables chosen. Figures 29 c), f), i), l) and o) show that there is a considerable fraction of CC1π^+1e events that don't get selected. Figure 29 c) shows that this seems to happen for high electron

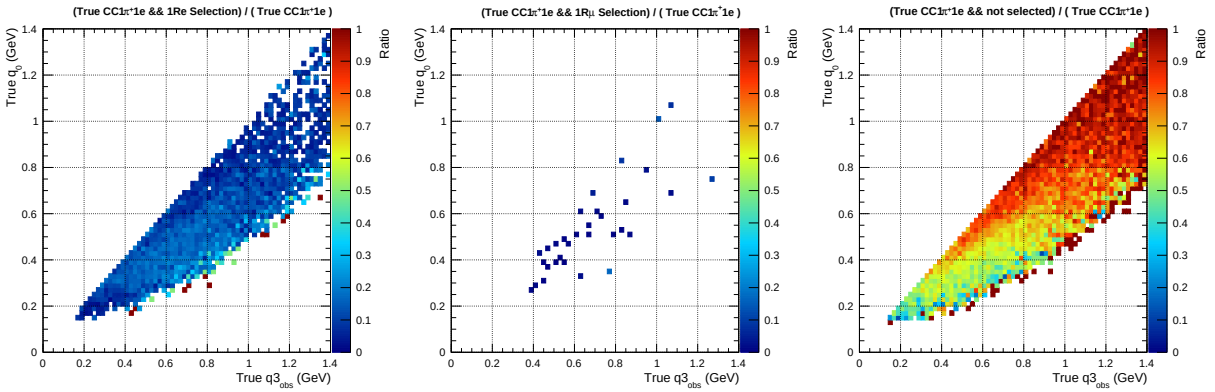

(j) True CC1π^+1e events passing 1Re selection in q_0 and q_3

(k) True CC1π^+1e events passing 1Rμ selection in q_0 and q_3

(l) True CC1π^+1e events passing no selection in q_0 and q_3

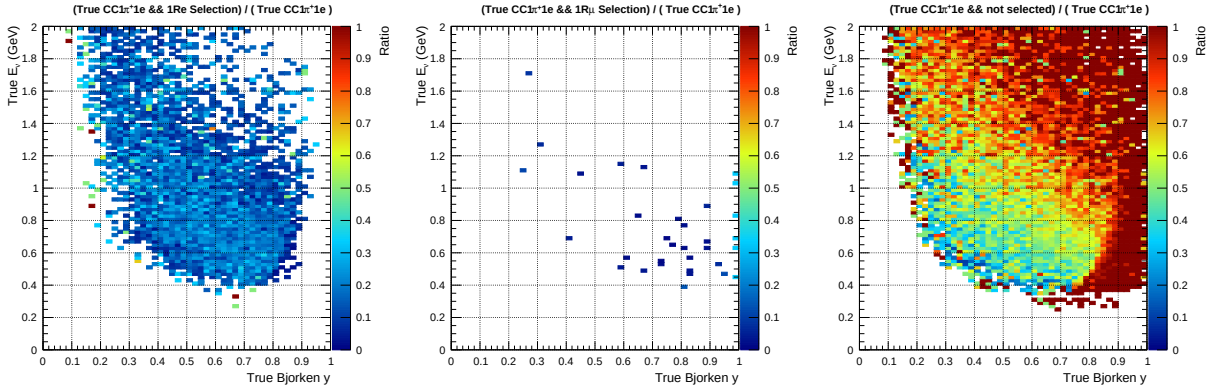

(m) True CC1π^+1e events passing 1Re selection in E_ν and y

(n) True CC1π^+1e events passing 1Rμ selection in E_ν and y

(o) True CC1π^+1e events passing no selection in E_ν and y

Figure 29: Mis-ID plots for true CC1π^+1e events in (p_l, $\cos\theta_{\nu l}$), (p_π, $\cos\theta_{\nu\pi}$), (q_0, W_{obs}), (q_0, q_3) and (E_ν, y)

momenta and 29 f) show that there appears to be a clear increase in the probability of not being selected at all with increased pion momentum which again could be associated with producing a second Cerenkov ring. It should be noted that the ν_eCC1π^+1e selection requires one decay electron however, the definition of true CC1π^+1e does not have a requirement for the number of decay electrons which could also be a cause of the seemingly low efficiency for true CC1π^+1e events.

4.3 Oscillated and Flux weighted acceptance maps

After receiving comments during a T2K-Analysis meeting, plots where oscillation weightings and flux weightings are also ap[plied. Acceptance maps where just oscsillation weights and just flux weights are also supplied in the appendices

4.4 Codebase

The code used to make the `TTree` containing the information in these acceptance maps as well as the plotting script can be found here: `https://github.com/clarenc3/t2k-nova-studies/tree/master/SK`. For any questions about the code or the study please contact: `e.atkin17@imperial.ac.uk`.

Appendices

A ND280 selection enumeration

The enumerations used in plotting follows that in `psyche` and `psycheEventModel/src/SampleId.hxx`, which can be found at `https://repo.nd280.org/viewvc/ND280/psyche/psycheEventModel/src/SampleId.hxx?revision=1.6&view=markup`. They follow

- No ND280 selection: 0 or ¡0
- FGD1 CC0π ν_μ FHC: 3
- FGD1 CC1π ν_μ FHC: 4
- FGD1 CCOther ν_μ FHC: 5
- FGD2 CC0π ν_μ FHC: 19
- FGD2 CC1π ν_μ FHC: 20
- FGD2 CCOther ν_μ FHC: 21
- FGD1 CC0π $\bar{\nu}_\mu$ RHC: 43
- FGD1 CC1π $\bar{\nu}_\mu$ RHC: 44
- FGD1 CCOther $\bar{\nu}_\mu$ RHC: 45
- FGD2 CC0π $\bar{\nu}_\mu$ RHC: 49
- FGD2 CC1π $\bar{\nu}_\mu$ RHC: 50
- FGD2 CCOther $\bar{\nu}_\mu$ RHC: 51
- FGD1 CC0π ν_μ RHC: 55
- FGD1 CC1π ν_μ RHC: 56

- FGD1 CCOther ν_μ RHC: 57
- FGD2 CC0π ν_μ RHC: 61
- FGD2 CC1π ν_μ RHC: 62
- FGD2 CCOther ν_μ RHC: 63